Use of Benzyl Functionalized Chiral Amines in the Development of Novel Cu^{II} and Ni^{II} dithiocarbamate complexes

Abstract

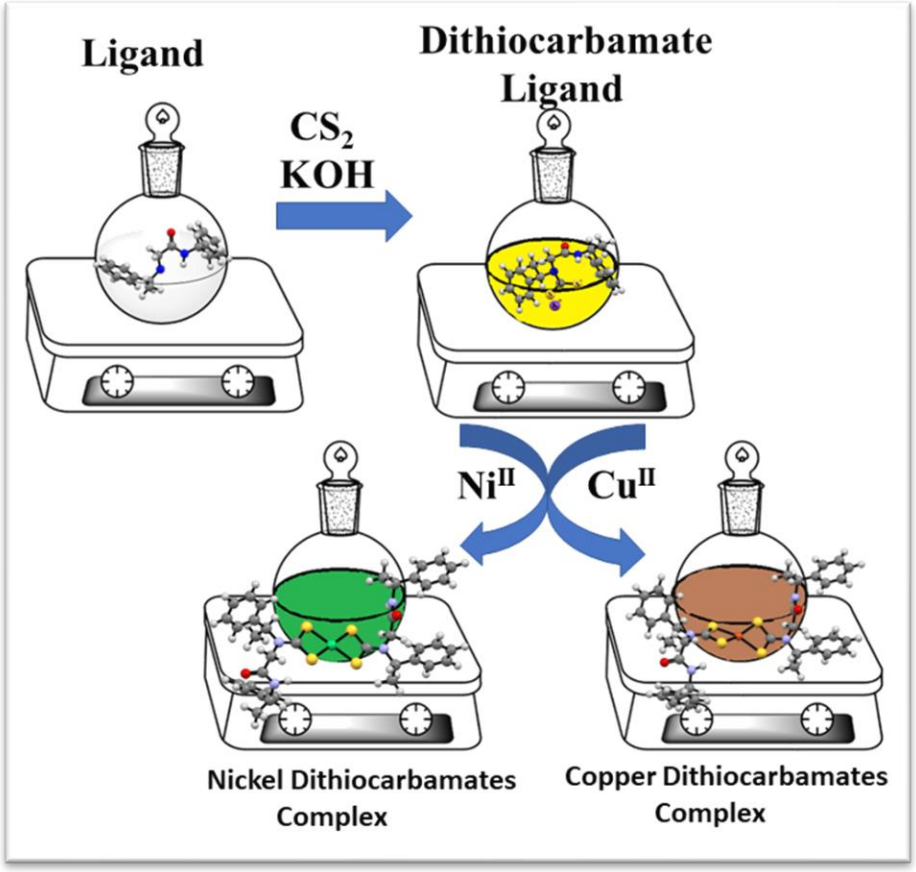

Organic chiral secondary amines such as (*S*,*S*)-2-(1-phenylethylamino)-*N*-(1-phenylethyl)acetamide (*S*,*S*-**L**^{1}), (*R*,*S*)-2-(1-phenylethylamino)-N-(1-phenylethyl)acetamide (*R*,*S*-**L**^{2}), (*R*,*R*)-2-(1-phenylethylamino)-N-(1-phenylethyl)acetamide (*R*,*R*-**L**^{3}) and (*S*,R)-2-(1-phenylethylamino)-N-(1-phenylethyl)acetamide (*S*,*R*- **L**^{4}), presented in chapter 5 were further derivatise into a new series of mononuclear M^{II}-dithiocarbamate complexes copper and nickel dithiocarbamate complexes *S*,*S*-**1**, *R*,*S*-**2**, *R*,*R*-**3**, *S*,*R*-**4**, *S*,*S*-**5**, *R*,*S*-**6**, *R*,*R*-**7**, *S*,*R*-**8**, holding chirality in the ligand skeleton. The composition and purity these complexes were confirmed by microanalysis and relevant spectroscopic techniques such as ^{1}H and ^{13}C NMR, FTIR, UV-visible. Magnetic susceptibility measurements along with UV-visible absorption study suggest square-planar/ distorted square-planar geometry

around the metal centres in all the complexes. The single crystal X-ray diffraction (SCXRD) technique has been used to determine the unprecedented molecular structure of *R*,*S*-**2**. SCXRD analysis revealed that the molecules of *R*,*S*-**2** adopts such a stereochemical conformations that opens an excessive number of weak intermolecular interactions, supported by mapping of MESP. The thermal stability and thermal degradation patterns of all the complexes were investigated by thermogravimetric analysis. A density functional theory calculation for all the newly synthesized complexes have been performed to reinforce the experimental outcomes. The non-conducting nature of the complexes has been verified with calculated HOMO-LUMO band gaps which falls in the range of 3.5-4.2 eV.

6.1 Introduction

The interest in the chemistry involving dithiocarbamate ligands has been continued due to the versatility of dithiocarbamates to construct a huge variety of inorganic-organic complex materials with fascinating physico-chemical properties. Transition metal complexes derived from dithiocarbamates have received a great deal of attention because of their interesting conducting properties, molecular magnetism, electrochemical, optoelectronic properties and biological applications.[1-3] The dithiocarbamate group is believed as a versatile pharmacophore since the discovery of first derivative dithiocarbamates *"*tetramethylthiuram disulfide (thiram)",[4] that has achieved prominence fungicidal properties and it is used in the compounds of biological interest.[5] The biological effects of transition metal containing dithiocarbamates centre as both pro-oxidant and antioxidant [6] along with their high metal-chelating capacity allows them to modulate the active sites of many metal-containing proteins. [7] Particularly, cancer cells have a high copper demand for their maintenance, proliferation and metastasis and thus copper dithiocarbamate complexes have shown potential in preclinical studies.[8] Although, the comprehensive molecular mechanisms of their anticancer activity remain largely unidentified, however, their mechanistic studies have shown that they can act as DNA intercalators, [9] inhibitors of nuclear factor kappa B (NF-κB), [10] proteasome inhibitors [11] and are also able to inactivate numerous metal-containing enzymes. [12]

Besides, the presence of metal-sulphur bond in these complexes enables them to serve as a synthetic precursor for the synthesis of metal sulphide nanoparticles.[13] The metal sulphide nanoparticles possess interesting properties such as electronic,

electrical magnetic and optical properties which make them useful in making sensors, photoconductors, catalysts for hydride nitrogen and hydro desulfurization, infrared detectors and solar cells.[14] Metal-sulphide nanoparticles are known to displays a number of phases that mainly depends on the reaction temperature, synthetic route adopted, and the nature of capping agents employed. The synthesis of diverse mineral phases of nickel sulphide nanoparticles with various capping agents have been reported. [15]

Moreover, thermogravimetric study has been successfully utilized to determine a widespread industrial application of dithiocarbamate compounds viz. reprocessing of polymers, fungicides, effective heat stabilizers, suitability dithiocarbamate complexes as single source precursor for the preparation of metal sulphide nano-particles and antioxidant action.[16] The cleavage of relatively weak C–S bonds provides a simple and tuneable route to pure phase materials of different stoichiometries and morphologies [17] during nanoscale synthesis of CuS and NiS. Additionally, dithiocarbamates themselves can act as capping agents and therefore they provide a physical barrier between interparticle interactions, preventing agglomeration that are particularly important during the optimization of nanoscopic properties of materials. [18] In particular, copper sulfides are widely studied as a result of their application in the diverse field of research viz optical filters, solar cells, photovoltaics, optical imaging and super-ionic materials. [19] Further a variety of stoichiometric phases ranging from copper-rich (Cu_2S) to sulfur-rich (CuS) phases with a phase-dependent direct/indirect bandgap in the range of 1.1–2.0 eV have been reported. [19]

Apart from thus, chirality has become an important part of nanoscience due to their distinct properties from those of the individual subunits or building blocks.[20] For instance, the chiral hybrid nanomaterials display potential applications in the area of asymmetric catalysis, selective separation, chiral sensing, and novel photonics. [21] A substantial progress in the nanoengineering of chiral composite nanomaterials has been made in the recent past. [22] A typical approach involved in the synthesis of chiral nanostructured materials uses organic chiral molecules such as designed peptides, [23] DNA, [24] surfactants, [25] sol−gel systems, [26] as template ligands along with inorganic counterparts.

Further reports suggests that chirality into nanostructured materials can be controlled deliberately either by employing different enantiomer templates [27] or by

the assistance of specific treatments. [28] For example, H. Lee et al. have employed amino-acids and peptides to guide the growth of chiral gold helicoids on a cubic or octahedral seed.[29] Chirality control for in Situ preparation of gold nanoparticle superstructures directed by a coordinatable organogelator has been reported by Zhao etal.[30] Another recent example of the directed growth of chiral nanoparticles was reported by G. Gonza´lez-Rubio et al.[31]

In the light of these observations, it was pertinent to use novel organic chiral amine precursors (*S,S*)-2-(1-phenylethylamino)-*N*-(1-phenylethyl)acetamide (*S,S*-**L^1**), (*R,S*)-2-(1-phenylethylamino)-N-(1-phenylethyl)acetamide (*R,S*-**L^2**), (*R,R*)-2-(1-phenylethylamino)-N-(1-phenylethyl)acetamide (*R,R*-**L^3**) and (*S*,R)-2-(1-phenylethylamino)-N-(1-phenylethyl)acetamide (*S,R*-**L^4**) (presented in Chapter **5**) in the synthesis of a new series of transition metal M^{II}-dithiocarbamate complexes *S,S*-**1,** *R,S*-**2,** *R,R*-**3,** *S,R*-**4,** *S,S*-**5,** *R,S*-**6,** *R,R*-**7,** *S,R*-**8** as per the Scheme 1 and to explore their potentials to be utilized suitably as a single source precursor for the development of metal-sulphide nanoparticles by using thermogravimetric analysis. Several experimental techniques viz ^{1}H and ^{13}C NMR, IR, UV-visible, SCXRD were used to characterize M^{II}-dithiocarbamate complexes and their compositions were verified by microanalysis. All the compounds were studied for their photophysical, thermal and electrochemical properties. Further, suitability of the M^{II}-dithiocarbamate complexes *S,S*-**1,** *R,S*-**2,** *R,R*-**3,** *S,R*-**4,** *S,S*-**5,** *R,S*-**6,** *R,R*-**7,** *S,R*-**8** as single source precursors for the development of meta-sulphide nano particles were verified by thermogravetric method.

6.2 Experimental and measurements

6.2.1 Materials and measurements

All solvents were purchased from the commercial sources and were freshly distilled prior to use. All the reagents such as $Cu(OAc)_2 \cdot H_2O$, $Ni(OAc)_2.4H_2O$ and CS_2 were purchased from Merck and Sigma-Aldrich Chemicals Limited, these were used without further purification. Elemental analyses (C, H, N) were carried out on a Perkin-Elmer 2400 analysers. Thin Layer Chromatography was performed on Merck 60 F254 Aluminium coated plates. FT-IR spectra were recorded in the 4000-400 cm^{-1} range using a Perkin-Elmer FT-IR spectrometer as KBr pellets. The ^{1}H and ^{13}C NMR spectra of relevant compounds were obtained on a Bruker AV-III 400 MHz spectrometer in spectrometer with DMSO-d_6 as solvent and TMS as internal standard.

UV-visible spectra were recorded on a JASCO V-730 UV-visible spectrophotometer. TGA/DTA plots were obtained using SII TG/DTA 6300 in flowing N_2 with a heating rate of 10 °C min^{-1}. Cyclic voltametric study was carried out on the CH instruments 600C potentiostat. Glassy carbon (BAS) is used as a working electrode, Ag/AgCl as a reference electrode and a Pt wire is used as a counter electrode. A 2.0 mM acetonitrile solution containing 0.2 M TBAP was analysed under a scan rate of 100 mVs^{-1}.

6.2.2 X-ray crystallography and data collection

Intensity data for Complex *R,S*-**2**·CH_3CN were collected on 'Xcalibur, Eos, Gemini' X-ray diffractometer equipped with Eos CCD detector at 298 K for [$C_{78}H_{87}N_9Ni_2O_4S_8$] in Monoclinic crystal system, MoKα (λ = 0.71073) radiation was used for the measurements. Data were collected and reduced by using the ''CrysAlisPro program.[32] An empirical absorption correction using spherical harmonics was implemented in ''SCALE3 ABSPACK'' scaling algorithm. The crystal structure was solved by direct methods using Olex2. [33] and the refinement was carried out against F^2 using SHELXL (Sheldrick, 2015) program. [34] All non-hydrogen atoms were refined anisotropically.

6.2.3 Computational method

All the calculations were carried out using the Gaussian 16 program suite and molecular orbitals were generated by GaussView 6.0 program.[35] Full geometry optimizations of complexes *S,S*-**1,** *R,S*-**2,** *R,R*-**3,** *S,R*-**4,** *S,S*-**5,** *R,S*-**6,** *R,R*-**7** and *S,R*-**8** have were performed using density functional theory (DFT) at B3LYP/LanL2DZ basis sets. This basis set has been used in a number of studies which showed good agreement with experimental results. A DFT level calculations were used to analyses frontier molecular orbitals, HOMO–LUMO energy gap and mapping of electrostatic potential surface to get insights of structural details of the complexes.

6.2.4 General synthetic procedure for M^{II}-dithiocarbamates *S,S*-**1,** *R,S*-**2,** *R,R*-**3,** *S,R*-**4,** *S,S*-**5,** *R,S*-**6,** *R,R*-**7** and *S,R*-**8**

To acetonitrile solution of 1 equivalent of respective organic chiral 2º amine precursor (*S,S*)-2-(1-phenylethylamino)-*N*-(1-phenylethyl)acetamide, *S,S*-$\mathbf{L^1}$ (0.282 g, 1mmol), (*R,S*)-2-(1-phenylethylamino)-N-(1-phenylethyl)acetamide, *R,S*- $\mathbf{L^2}$ (0.282 g, 1mmol), (*R,R*)-2-(1-phenylethylamino)-N-(1-phenylethyl)acetamide, *R,R*-$\mathbf{L^3}$ (0.282 g, 1mmol) or (*S,*R)-2-(1-phenylethylamino)-N-(1-phenylethyl)acetamide, *S,R*- $\mathbf{L^4}$ (0.282 g, 1mmol) an excess amount of NaOH (~3 equivalent; ~ 0.120 g) and carbon disulfide

(~10 equivalent; ~ 0.4 ml) were added with vigorous stirring. The mixture was stirred further for 12 hours at room temperature. A change in colour from colourless to pale yellow was observed during the progress of a reaction. To this reaction mixture, $Ni(OAc)_2.4H_2O$ (124 mg, 0.5 mmol) or $Cu(OAc)_2$. H_2O (0.100 g, 0.5 mmol) was dissolved in a minimum amount of distilled water, was added with rigorous stirring and the reaction was allowed to continue for 8 h at room temperature. The reaction mixture was concentrated on rotatory evaporator leaving the greenish color or brown residue. The residue was filtered, washed with distilled water (5ml × 2 times) followed by petroleum ether (5ml × 3 times) and dried under high vacuum to give the products in 85-90 % yield. The overall reaction is outlined in Scheme1. The green solid or brown solid products were stored under nitrogen and data were collected.

Table 1. Micro-, mass- and IR analysis data for compounds *S,S*-**1,** *R,S*-**2,** *R,R*-**3,** *S,R*-**4,** *S,S*-**5,** *R,S*-**6,** *R,R*-**7** and *S,R*-**8.**

Entry	Molecular Formula	Molecular Weight	Yield (%)	MP/BP (°C)	Elemental Analysis % Found (calculated)			IR data (KBr disc) υ_{max}/cm^{-1}
					C	H	N	
S, S-**1**	$C_{38}H_{42}N_4NiO_2S_4$	773	86	>250	59.21 (58.99)	6.61 (5.47)	7.87 (7.24)	3298(N-H), 2973(C-H), 1662(C=O), 1531, 1471, 1241, 1159, 964, 759, 698, 534
R, S-**2**	$C_{38}H_{42}N_4NiO_2S_4$	773	85	>250	59.65 (58.99)	6.53 (5.47)	7.57 (7.24)	3288(N-H), 2980(C-H), 1657(C=O), 1544, 1470, 1247, 1160, 965, 784, 669, 560
R, R-**3**	$C_{38}H_{42}N_4NiO_2S_4$	773	89	>250	59.19 (58.99)	6.26 (5.47)	7.87 (7.24)	3293(N-H), 2975(C-H), 1663(C=O), 1532, 1465, 1242, 1162, 966, 753, 698, 538
S, R-**4**	$C_{38}H_{42}N_4NiO_2S_4$	773	90	>250	59.35 (58.99)	6.50 (5.47)	7.81 (7.24)	3288(N-H), 2972(C-H), 1659(C=O), 1538, 1471, 1241, 1160, 965, 761, 698, 536
S, S-**5**	$C_{38}H_{42}N_4CuO_2S_4$	778	87	>250	59.35 (58.62)	6.50 (5.44)	7.81 (7.20)	3288(N-H), 2972(C-H), 1659(C=O), 1538, 1471, 1241, 1160, 966, 761, 698, 536
R, S-**6**	$C_{38}H_{42}N_4CuO_2S_4$	778	85	>250	59.38 (58.62)	6.70 (5.44)	7.85 (7.20)	3296(N-H), 2973(C-H), 1662(C=O), 1548, 1471, 1254, 1163, 967, 752, 698, 540
R, R-**7**	$C_{38}H_{42}N_4CuO_2S_4$	778	89	>250	59.40 (58.62)	6.67 (5.44)	7.28 (7.20)	3293(N-H), 2974(C-H), 1657(C=O), 1539, 1451, 1244, 1157, 963, 762, 698, 540
S, R-**8**	$C_{38}H_{42}N_4CuO_2S_4$	778	90	>250	59.99 (58.62)	5.47 (5.44)	7.24 (7.20)	3287(N-H), 2974(C-H), 1661(C=O), 1549, 1454, 1206, 1163, 966, 749, 697, 537

Table 2. NMR spectral data for compounds *S*,*S*-**1,** *R*,*S*-**2,** *R*,*R*-**3** and *S*,*R*-**4**.

Entry	**NMR Data (ppm)**	
	^{1}H NMR (DMSO d_6)	**^{13}C NMR (DMSO d_6)**
S, S-**1**	8.41 (s, 2H, -N*H*CO); 7.20-7.45 (m, 20H, *Bz*); 5.80 (m, 2H, -C*H*); 4.84 (q, 2H, -C*H*); 4.24 (d, 2H, -CH_2CO); 3.89 (d, 2H, -CH_2CO); 1.48 (d, 6H, -CH_3); 1.27 (d, 6H, -CH_3).	208.1, 164.5, 144.7, 144.4, 138.4, 129.2, 128.7, 127.3, 126.4, 57.7, 48.6, 48.2, 22.9, 16.4.
R, S-**2**	8.43 (s, 2H, -N*H*CO); 7.24-7.41 (m, 20H, *Bz*); 5.80 (m, 2H, -C*H*); 4.84 (q, 2H, -C*H*); 4.24 (d, 2H, -CH_2CO); 4.16 (d, 2H, -CH_2CO); 1.55 (d, 6H, -CH_3); 1.29 (d, 6H, -CH_3).	208.2, 165.0, 144.4, 138.5, 129.2, 128.5, 127.5, 126.4, 57.7, 48.6, 48.2, 22.9.
R, R-**3**	8.41 (s, 2H, -N*H*CO); 7.22-7.45 (m, 20H, *Bz*); 5.80 (m, 2H, -C*H*); 4.84 (q, 2H, -C*H*); 4.24 (d, 2H, -CH_2CO); 3.89 (d, 2H, -CH_2CO); 1.48 (d, 6H, -CH_3); 1.27 (d, 6H, -CH_3).	212.8, 175.4, 169.2 149.7, 143.2, 133.6, 131.9, 131.7, 131.0, 61.9, 53.4, 52.9, 27.8, 21.9.
S, R-**4**	8.41 (s, 2H, -N*H*CO); 7.19-7.44 (m, 20H, *Bz*); 5.80 (m, 2H, -C*H*); 4.86 (q, 2H, -C*H*); 4.24 (d, 2H, -CH_2CO); 4.17 (d, 2H, -CH_2CO); 1.56 (d, 6H, -CH_3); 1.31 (d, 6H, -CH_3).	208.1, 164.5, 144.7, 144.3, 138.5, 129.2, 128.6, 127.1, 126.4, 57.2, 48.5, 48.1, 22.7, 16.4.

6.3 RESULTS AND DISCUSSION

6.3.1 Synthesis and Characterization

A single pot reaction involving self-assembling of *S,S*-**L^1**, *R,S*-**L^2**, *R,R*- **L^3** or *S,R*- **L^4** with CS_2 and $Ni(OAC)_2.4H_2O$ or $Cu(OAC)_2.H_2O$ in CH_3CN affords access to a series of amide functionalized transition metal M^{II}-dithiocarabamte complexes of the type $[M\{\kappa^2S,S\text{-}S_2CN(CH(R/S\text{-}CH_3)Ph)(CH_2CONH(CH(R/S\text{-}CH_3)Ph)\}_2]$ (M= Ni^{II} , *S,S*-**1,** *R,S*-**2,** *R,R*-**3**, *S,R*-**4**; M= Cu^{II}, *S,S*-**5,** *R,S*-**6,** *R,R*-**7** and *S,R*-**8**) in good yields by following the Scheme 1. After workup the products were obtained as green (in case of nickel) and brown (in case of copper) solids in 85−90% isolated yield. These complexes are reasonably soluble in common organic solvents viz. ethyl acetate, methanol, acetonitrile etc and stable in the solution for long times.

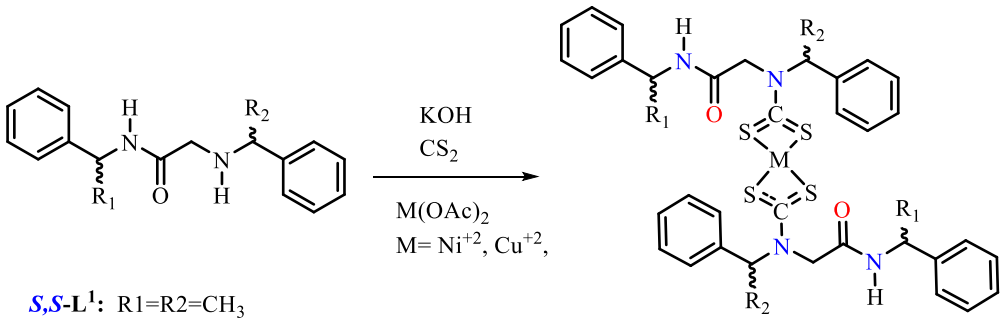

***S,S*-L^1:** R1=R2=CH_3
***R,S*-L^2:** R1= R2=CH_3
***R,R*-L^3:** R1=R2=CH_3
***S,R*-L^4:** R^1=R^2=CH_3

***S,S*-1**: R1 = R2 = CH_3, M = Ni^{+2} ; ***R,S*-2**: R1 = R2 = CH_3 , M = Ni^{+2}
***R,R*-3**: R1 = R2 = CH_3, M = Ni^{+2} ; ***S,R*-4**: R1 = R2 = CH_3, M = Ni^{+2}
***S,S*-5**: R1 = R2 = CH_3, M = Cu^{+2} ; ***R,S*-6**: R1 = R2 = CH_3, M = Cu^{+2}
***R,R*-7**: R1 = R2 = CH_3, M = Cu^{+2} ; ***S,R*-8**: R1 = R2 = CH_3, M = Cu^{+2}

Scheme 1. General synthetic strategies adopted for chiral mononuclear Cu^{II}- and Ni^{II}-dithiocarbamate complexes *S,S*-**1,** *R,S*-**2,** *R,R*-**3,** *S,R*-**4,** *S,S*-**5,** *R,S*-**6,** *R,R*-**7** and *S,R*-**8.**

The compositions and phase purity of the samples were confirmed by microanalysis and by ^1H and ^{13}C spectroscopy. The NMR (Annexure 1-8) and IR spectra (Annexure 9-16) gives confirmation of various groups viz. methine, methylene, amino- amido- and phenyl groups in the diamagnetic compounds *S,S*-**1,** *R,S*-**2,** *R,R*-**3,** *S,R*-**4.** The assignments of IR and NMR data are summarized in the experimental section under Table 1 and Table 2. Chiral methine protons appear ~ 4.84 ppm and 5.80 ppm and amidic protons appear in the range of 8.41-8.43 ppm in the ^1H NMR spectrum of diamagnetic complexes. The ^1H NMR spectral study is well supported by the corresponding ^{13}C NMR. The most characteristic ^{13}C NMR signals of diamagnetic Ni^{II}-dithiocarbamate complexes *S,S*-**1,** *R,S*-**2,** *R,R*-**3,** *S,R*-**4** appeared in

a highly downfield region at ~ 208 ppm due to coordinated dithiocarbamate (-NCS_2) moieties. The IR spectra of all the complexes gave characteristic bands at ~3000 cm^{-1} due to the υ(C-H) stretching frequency and at ~1660 cm^{-1} due to the υ(C=O) stretching frequency of the amide group. Notably, the IR spectrum of the complexes *S,S*-**1,** *R,S*-**2,** *R,R*-**3,** *S,R*-**4,** *S,S*-**5,** *R,S*-**6,** *R,R*-**7** and *S,R*-**8** gave two new single sharp medium intensity bands in the 1471-1465 cm^{-1} and 966-963 cm^{-1} regions, attributable to ν(N-CS_2) and ν(C-S) stretching frequencies, associated with the symmetric bidentate dithiocarbamate lignads. The NMR and IR spectral values are found to be consistent with the literature.[36]

The UV-visible absorption spectrum of M^{II}-dithiocarbamates complexes apparently display a high intensity band in the 250-280 nm regions and a medium intensity band in 297-330 nm regions, attributable to the locally excited π→ π* and n→π* intra-ligand transitions. A low intensity band in 395-438 nm region ligand to ligand→metal charge transfer transitions, a characteristicfeature of coordinated dithiocarbamate (NCS_2) ligands. **(**Figure 1a and Figure 1b**)** Additionally, Cu^{II}-dithiocarbamates complexes *S,S*-**5,** *R,S*-**6,** *R,R*-**7** and *S,R*-**8** gave a very weak absorption band at ~ 630 nm which can be attributed to d-d transition band. The magnetic moment values (Table 3) along with UV-visible absorption bands suggest the square planar/ distorted square planar environment[26] around Ni^{II}/ Cu^{II} centres in M^{II}-dithiocarbamates.[37]

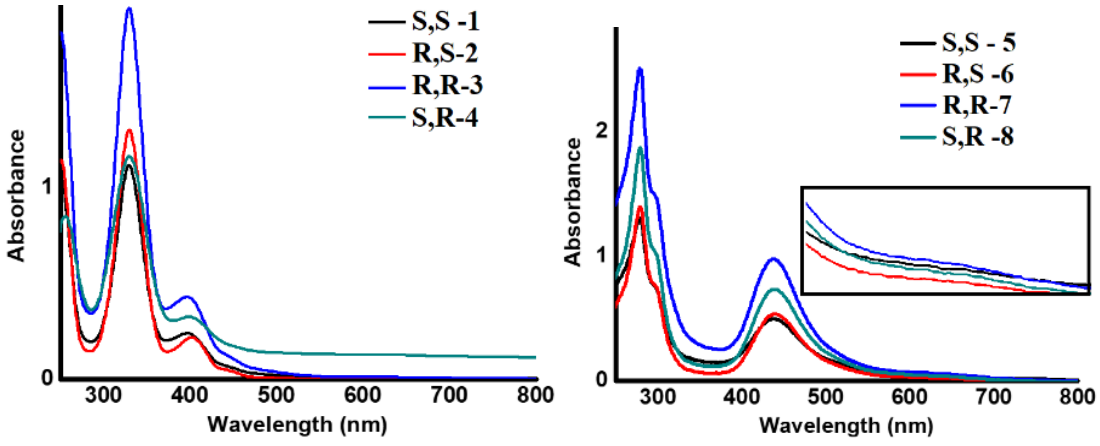

Figure 1. The UV-visible spectral data of (a) N^{II}-dithiocarbamate complexes *S,S*-**1,** *R,S*-**2,** *R,R*-**3,** *S,R*-**4** and (b) N^{II}-dithiocarbamate complexes *S,S*-**5,** *R,S*-**6,** *R,R*-**7** and *S,R*-**8**.

Table 3. UV-visible spectral data of ligand precursors and complexes 10^{-4} M in $CHCl_3$

Entry	λ_{max} nm (10^{-4}M, ε L Mol^{-1} cm^{-1})	Magnetic Moment μeff (BM)
S,S-**1**	252 (10400) π→ π*, 330 (11600) n→π*, 404 (1948) CT	diamagnetic
R,S-**2**	253 (11217) π→ π*, 329 (13018) n→π*, 402 (2183) CT	diamagnetic
R,R-**3**	255 (8500) π→ π*, 329 (11630) n→π*, 400 (03290) CT	diamagnetic
S,R-**4**	256 (10200) π→ π*, 328 (23110) n→π*, 395 (4332) CT	diamagnetic
S,S-**5**	280 (13123) π→ π*, 298 (7351) n→ π*, 436 (5016) CT, 637 (1179) d-d transition.	1.84
R,S-**6**	278 (14004) π→ π*, 297 (7646) n→ π*, 437 (5216) CT, 637 (1198) d-d transition.	1.87
R,R-**7**	275 (15101) π→ π*, 297 (7715) n→ π*, 438 (5311) CT, 638 (1234) d-d transition.	1.94
S,R-**8**	273 (13264) π→ π*, 298 (7454) n→ π*, 437(5165) CT, 637 (1146) d-d transition.	1.91

6.3.2 Thermogravimetric Analysis

Thermal stability, thermal degradation patterns and the rate of degradation of all the M^{II}-dithiocarbamate complexes *S,S*-**1,** *R,S*-**2,** *R,R*-**3,** *S,R*-**4,** *S,S*-**5,** *R,S*-**6,** *R,R*-**7** and *S,R*-**8** were investigated by performing thermogravimetric study. The heating rate was suitably guarded at 10° C min^{-1} under nitrogen atmosphere. The outcomes of are thermogravimetric study are presented in Figure 2 and Figure 3. The temperature dependent mass losses, rate of thermal decomposition and the residual masses corresponding to final degradation products are tabulated in Table 4. Evidently, all the complexes are stable up to 200 °C without any mass loss on TGA curves and their degradation essentially takes place in a single stage. Notably, the thermal stability of Ni^{II}-dithiocarbamate complexes *S,S*-**1,** *R,S*-**2,** *R,R*-**3,** *S,R*-**4** are considerably higher than the analogous Cu^{II}-dithiocarbamate complexes *S,S*-**5,** *R,S*-**6,** *R,R*-**7** and *S,R*-**8**. Interestingly, all of the Cu^{II}-dithiocarbamate complexes *S,S*-**5,** *R,S*-**6,** *R,R*-**7** and *S,R*-**8** undergo a single stage of mass loss on DTG curves with a maximum rate of mass loss at 267 °C, 245 °C, 277 °C and 264 °C respectively, and all the complexes gave a stable residual mass of 13.7 %, 13.3 %, 13.4 %, and 13.1 %,respectively on TG curves which corresponds to CuS. However, residual mass obtained for analogous Ni^{II}-dithiocarbamate complexes *S,S*-**1,** *R,S*-**2,** *R,R*-**3,** *S,R*-**4** on TG curves corresponds to CuS plus char.

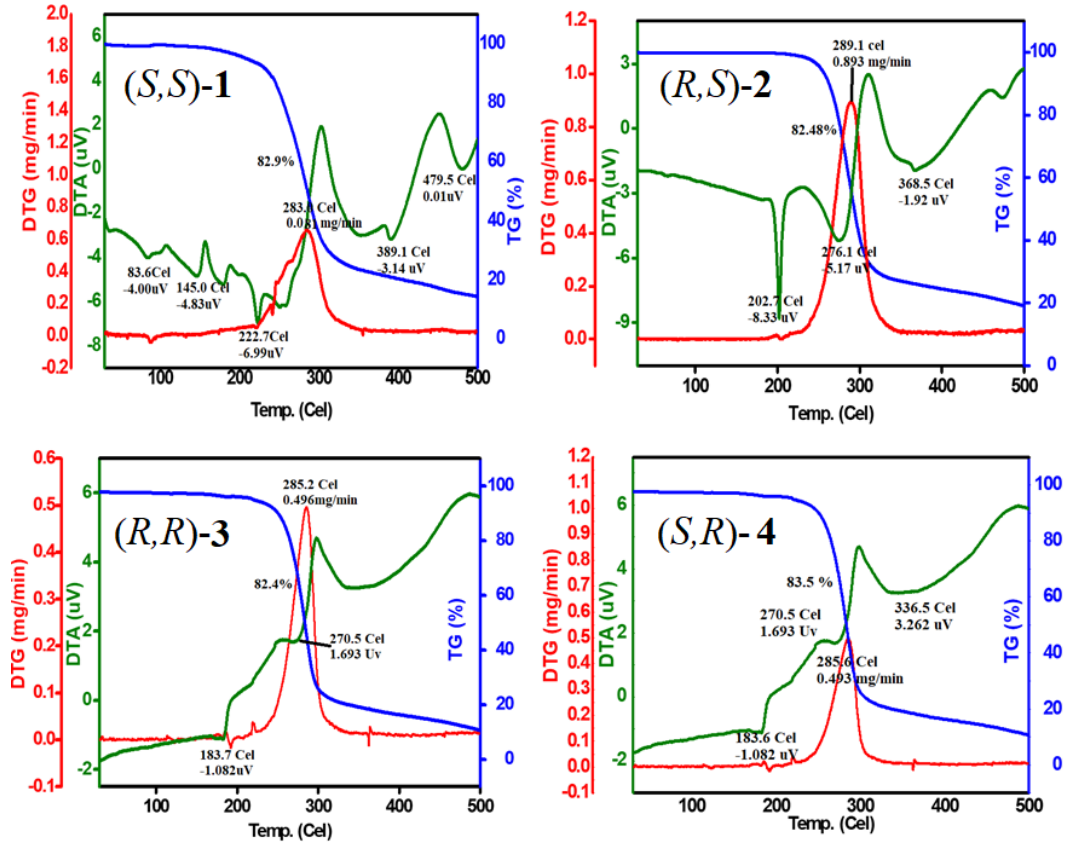

Figure 2. TG/DTA curves for the nickel complexes *S*,*S*-**1,** *R*,*S*-**2,** *R*,*R*-**3** and *S*,*R*-**4**.

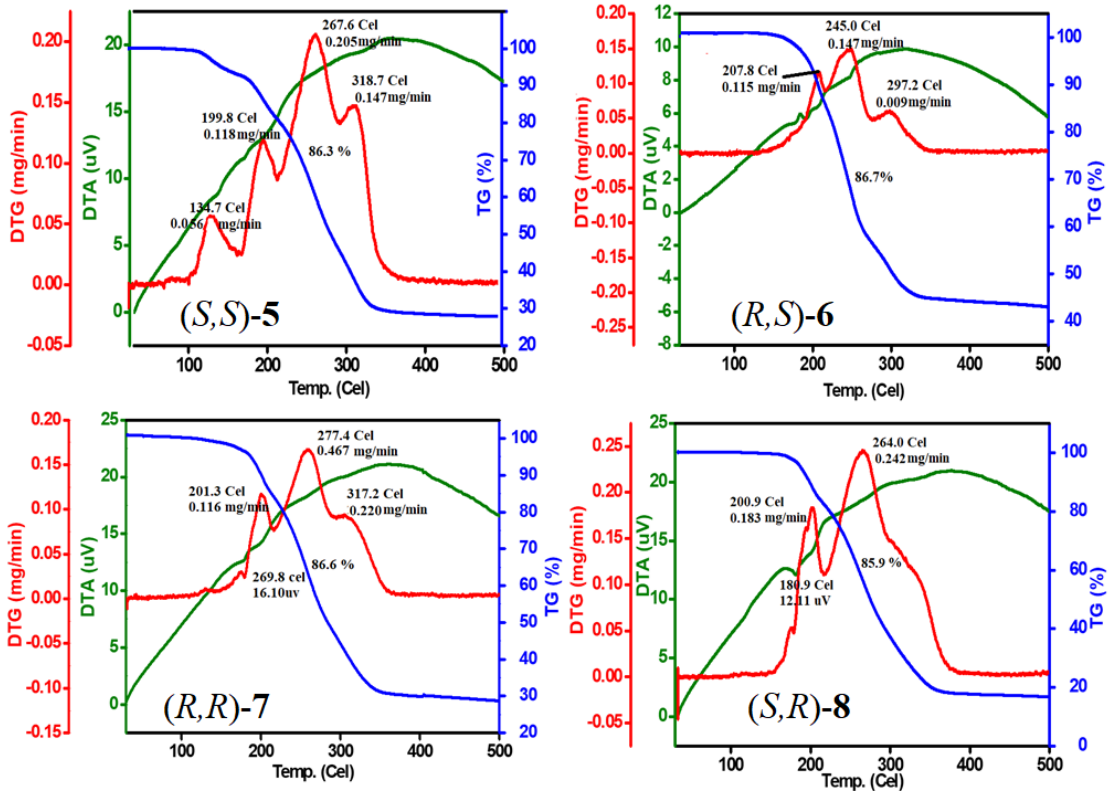

Figure 3. TG/DTA curves for the copper complexes *S*,*S*-**5,** *R*,*S*-**6,** *R*,*R*-**7** and *S*,*R*-**8**.

Table 4. Thermal analysis data of the mononuclear M^{II}-dithiocarbamate complexes.

Entry	% Mass loss (Temp. range °C)	DTG (°C) (mg min^{-1})	% Residue Calculated (found)	Theoretical % of NiS	Final product
S,*S*-**1**	82.9 (200-300)	283.0 (0.081)	17.1	11.6	NiS + char
R,*S*-**2**	82.5 (200-300)	289.1 (0.893)	17.5	11.6	NiS + char
R,*R*-**3**	82.4 (200-300)	285.2 (0.496)	17.6	11.6	NiS + char
S,*R*-**4**	83.5 (200-300)	285.6 (0.493)	16.5	11.6	NiS + char
S,*S*-**5**	86.3 (200-300)	267.6 (0.205)	13.7	12.2	CuS
R,*S*-**6**	86.7 (200-300)	245.0 (0.147)	13.3	12.2	CuS
R,*R*-**7**	86.6 (200-300)	277.4 (0.467)	13.4	12.2	CuS
S,*R*-**8**	85.9 (200-300)	264.0 (0.242)	14.1	12.2	CuS

Thermogravimetric study performed on all the complexes clearly suggests the potentials of these compounds to serve as a single source precursor for the synthesis of metal-sulfide nanoparticles which finds various applications in the diversified area of research.[14, 19] Of more interesting, the presence of chirality in the ligand backbone of these complexes would facilitate a fine tuning of size and shape of resulting nanoparticles. Reports suggests that chirality into nanostructured materials can be controlled consciously either by employing different enantiomer templates or by the assistance of specific treatments (vide supra). The chiral hybrid nanomaterials are known to display several applications in the area of asymmetric catalysis, selective separation, chiral sensing, and novel photonics. [21]

6.3.3 X-ray crystallographic study

Single crystals of Ni^{II}-dithiocarbamate complex *R*,*S*-**2** suitable for single crystal X-ray diffraction (SCXRD) study were grown by slow evaporation of ethyl acetate solution at 4° C temperature. The molecules of complex *R*,*S*-**2** crystallized in monoclinic $P2_1$ space group. The X-ray crystal structure of this complex *R*,*S*-**2** shows two of the molecule of $[C_{78}H_{87}N_9Ni_2O_4S_8]$ in its asymmetric unit as shown in Figure 4a. There are four such units in the unit cell (Figure 4b). Information about data collection, refinement, and structure solution are recorded in (Table 5). The structural parameters for Ni^{II}-dithiocarbamate complex *R*,*S*-**2** are found in the normal range.[37]

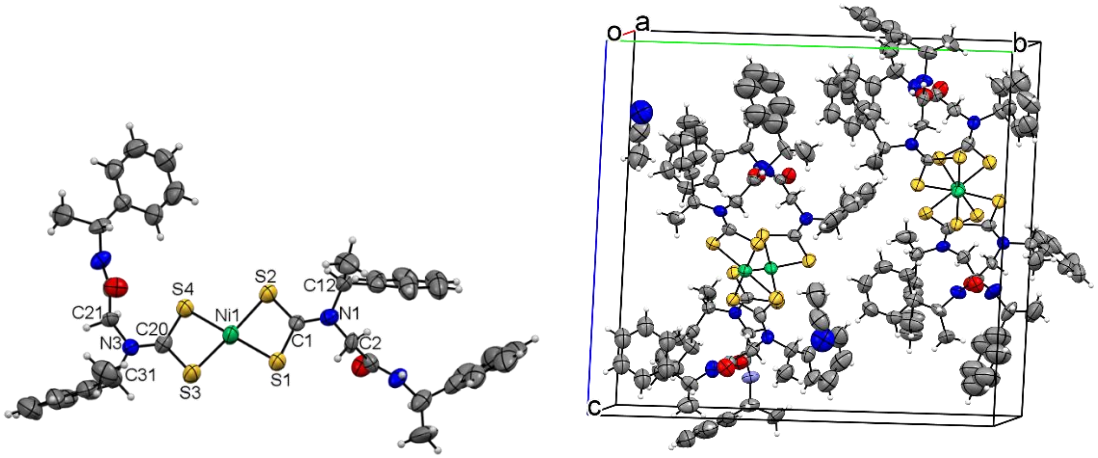

(a) **(b)**

Figure 4. (a) The *ORTEP* diagram of complex *R*,*S*-**2** with 50% probability and partial numbering scheme (b) presence of four molecules per unit cell.

Table 5. Crystal data and structure refinement for the complex *R*,*S*-**2**.CH_3CN under investigation.

Identification code	*R*,*S*-**2** .CH_3CN
Empirical formula	$C_{78}H_{87}N_9Ni_2O_4S_8$
Formula weight	1588.47
Temperature/K	293
Crystal system	monoclinic
Space group	$P2_1$
a/Å	9.5774(6)
b/Å	21.6228(9)
c/Å	19.9314(9)
α/°	90
β/°	101.866(5)
γ/°	90
Volume/Å^3	4039.4(4)
Z	2
ρ_{calc}mg/mm^3	1.306
μ/mm^{-1}	0.726
F(000)	1668
2Θ range for data collection	6.42 to 50.8°
Index ranges	$-10 \le h \le 10$, $-23 \le k \le 23$, $-21 \le l \le 21$
Reflections collected	30060
Independent reflections	10390[R(int) = 0.0910]
Data/restraints/parameters	10390/8/859
Goodness-of-fit on F^2	0.913
Final R indexes [I>=2σ (I)]	R_1 = 0.0668, wR_2 = 0.1502
Final R indexes [all data]	R_1 = 0.1149, wR_2 = 0.1899
Largest diff. peak/hole / e Å^{-3}	0.70/-0.29
Flack parameter	0.02(2)

In Ni^{II}-dithiocarbamate complexe *R*,*S*-**2**, Ni(II) center is bonded to the four soft sulphur sites of dithiocarbamate ligands (prepared *in situ*) and adopted square-planar geometry with coplanar chelate rings involving Ni1S1S2C1 and Ni1S3S4C20 atoms (Figure 4a). The average Ni-S, C-S and N-C bond distances are 2.2 Å, 1.70 Å and 1.32 Å respectively. The average bite angle S-Ni-S is 79.19 ° while diagonal angle S-Ni-S is 173.8°. The selected structural parameters are tabulated in Table 6. The structural parameters obtained experimentally matches well with the similar parameters reported in the literature[37] as well as theoretically determined parameters, discussed later.

Table 6. Selected bond length and bond angle of Ni^{II}-dithiocarbamate complexe R,S-2.

Code	Selected Bond	Bond Length(Å)	Selected Bond	Bond angle (°)
R,*S*-**2**	Ni1-S1	2.202(3)	S1-Ni1-S2	79.19(10)
	Ni1-S2	2.199(3)	C1-S1-Ni1	84.8(3)
	S1-C1	1.716(10)	C1-S2-Ni1	85.4(3)
	S2-C1	1.697(9)	S1-Ni1-S4	176.94(13)
	C1-N1	1.321(11)	S2-Ni1-S3	173.75(14)
	N1-C12	1.482(12)	S1-C1-S2	110.6(5)
			S1-C1-N1	124.7(7)
			S2-C1-N1	124.8(7)

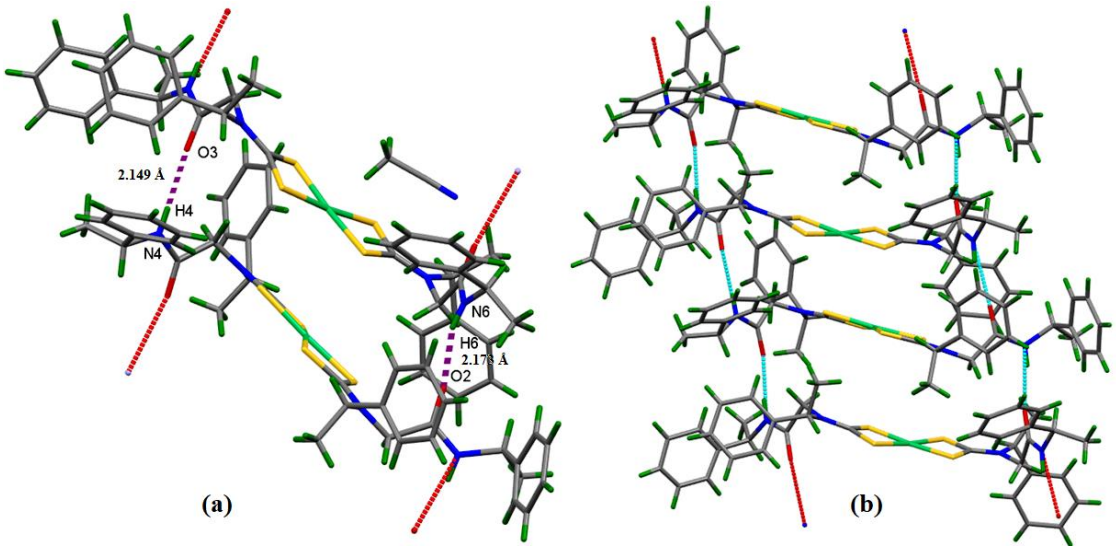

Figure 5. (a) Asymmetric molecules of *R*,*S*-**2** forming a hydrogen bonding closing contacts (b) formation of a fascinating ladder like architecture alond a-axis by the molecules of *R*,*S*-**2.**

Notably, the two molecules present in the asymmetric unit are interconnected with a N4-H4…O3 (2.149 Å) and N6-H6…O2 (2.173 Å) closing hydrogen bonding

contacts (Figure 5a) and these contacts are extend along *a*-axis, forming a fascinating ladder like architecture as shown in the Figure 5b. Overall, the molecules of *R*,*S*-**2** are associated with an excessive number of weak intermolecular interactions and stabilize the molecules in the solid state.

6.3.4 Density functional theory calculations

A DFT level calculations and full geometry optimization of Complexes *S*,*S*-**1,** *R*,*S*-**2,** *R*,*R*-**3,** *S*,*R*-**4,** *S*,*S*-**5,** *R*,*S*-**6,** *R*,*R*-**7** and *S*,*R*-**8** have been executed using B3LYP/6-31G and B3LYP/LanL2DZ basis sets respectively. The structural parameters such as bond lengths and bond angles obtained theoretically for compounds *S*,*S*-**1,** *R*,*S*-**2,** *R*,*R*-**3,** *S*,*R*-**4,** *S*,*S*-**5,** *R*,*S*-**6,** *R*,*R*-**7** and *S*,*R*-**8** were found to be consistent with the similar parameters obtained experimentally by X-ray study of closely related compounds.[37] Further, the bond lengths and bond angles determined experimentally by means single crystal XRD (Table 6) for compound *R*,*S*-**2** are comparable with the similar parameters (Table 7) calculated at B3LYP/LanL2DZ level and thus it validate the method of optimization. An optimized geometry for the minimum energy conformation of Ni^{II}-dithiocarbamates *S*,*S*-**1,** *R*,*S*-**2,** *R*,*R*-**3** and *S*,*R*-**4** along with Cu^{II}-dithiocarbamates *S*,*S*-**5,** *R*,*S*-**6,** *R*,*R*-**7** and *S*,*R*-**8** are provided in Figure 6. Energy of optimized geometry and HOMO-LUMO gaps for all the compounds are summarized in Table 8.

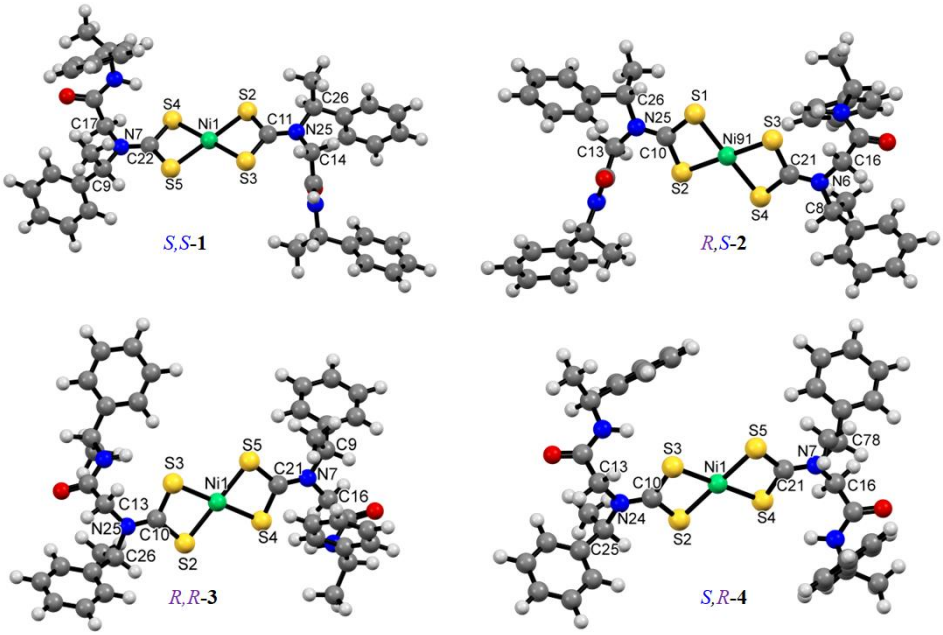

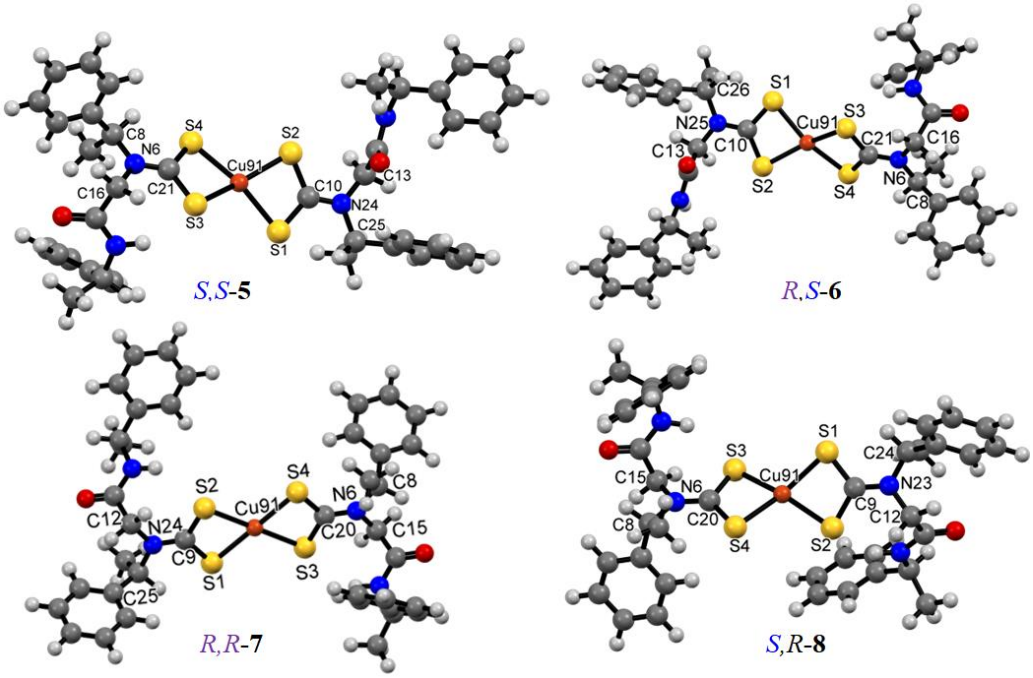

Figure 6: An optimized geometry for the minimum energy conformation of Copper DithioCarbamates Complexes *S*,*S*-**1,** *R*,*S*-**2,** *R*,*R*-**3,** *S*,*R*-**4,** *S*,*S*-**5,** *R*,*S*-**6,** *R*,*R*-**7** and *S*,*R*-**8** at B3LYP/LanL2DZ level.

Table 7: Theoretical value of bond lengths (Å) and average bond angles (º) obtained by DFT calculatons for *S*,*S*-**1,** *R*,*S*-**2,** *R*,*R*-**3,** *S*,*R*-**4,** *S*,*S*-**5,** *R*,*S*-**6,** *R*,*R*-**7** and *S*,*R*-**8**.

Code	Selected Bond	Average Bond Length(Å)	Selected Bond	Average Bond angle (º)
S,*S*-**1**	Ni1-S2 Ni1-S3 S2-C11 S3-C11 C11-N25 N25-C14 N25-C26	2.299 2.299 1.782 1.781 1.336 1.469 1.515	S2-Ni1-S3 C11-S2-Ni1 C11-S3-Ni1 S2-Ni1-S5 S3-Ni1-S4 S2-C11-S3 S2-C11-N25	80.34 83.47 83.59 178.38 179.06 112.57 124.33
R,*S*-**2**	Ni91-S1 Ni91-S2 S1-C10 S2-C110 C10-N25 N25-C13 N25-C26	2.296 2.295 1.783 1.781 1.335 1.469 1.515	S1-Ni91-S2 C10-S1-Ni91 C10-S2-Ni91 S1-Ni91-S4 S2-Ni91-S3 S1-C10-S2 S1-C10-N25	80.36 83.48 83.60 177.43 179.40 112.54 124.32
R,*R*-**3**	Ni1-S2 Ni1-S3 S2-C10 S3-C10 C11-N25 N25-C13 N25-C26	2.299 2.294 1.782 1.795 1.336 1.485 1.524	S2-Ni1-S3 C10-S2-Ni1 C10-S3-Ni1 S2-Ni1-S5 S3-Ni1-S4 S2-C10-S3 S2-C10-N25	80.27 84.01 83.89 179.58 179.74 111.71 124.65
S,*R*-**4**	Ni1-S2	2.301	S2-Ni1-S3	80.25

	Ni1-S3	2.294	C10-S2-Ni1	83.96
	S2-C10	1.781	C10-S3-Ni1	83.89
	S3-C10	1.795	S2-Ni1-S5	179.60
	C10-N24	1.334	S3-Ni1-S4	179.82
	N24-C13	1.484	S2-C10-S3	111.78
	N25-C25	1.522	S2-C10-N24	124.76
S,*S*-**5**	Cu91-S1	2.381	S1- Cu91-S2	78.71
	Cu91-S2	2.383	C10-S1- Cu91	82.90
	S1-C10	1.789	C10-S2- Cu91	83.01
	S2-C10	1.786	S1- Cu91-S4	159.04
	C10-N24	1.338	S2- Cu91-S3	160.90
	N24-C13	1.469	S1-C10-S2	115.36
	N24-C25	1.516	S2-C10-N24	122.92
R,*S*-**6**	Cu91-S1	2.318	S1- Cu91-S2	78.66
	Cu91-S2	2.316	C10-S1- Cu91	82.86
	S1-C10	1.738	C10-S2- Cu91	83.01
	S2-C10	1.735	S1- Cu91-S4	159.24
	C10-N25	1.339	S2- Cu91-S3	159.36
	N25-C13	1.460	S1-C10-S2	115.46
	N25-C26	1.497	S1-C10-N25	122.89
R,*R*-**7**	Cu91-S1	2.441	S1- Cu91-S2	76.84
	Cu91-S2	2.453	C10-S1- Cu91	85.31
	S1-C9	1.796	C10-S2- Cu91	84.85
	S2-C9	1.801	S1- Cu91-S4	154.46
	C9-N24	1.309	S2- Cu91-S3	154.05
	N24-C12	1.479	S1-C9-S2	113.81
	N24-C25	1.515	S2-C9-N24	122.73
S,*R*-**8**	Cu91-S1	2.384	S1- Cu91-S2	78.52
	Cu91-S2	2.383	C9-S1- Cu91	83.35
	S1-C9	1.788	C9-S2- Cu91	83.63
	S2-C9	1.800	S1- Cu91-S4	161.37
	C9-N23	1.336	S2- Cu91-S3	160.80
	N23-C12	1.485	S1-C9-S2	114.43
	N23-C24	1.524	S2-C9-N23	123.35

The analysis of frontier molecular orbitals of M^{II}-dithiocarbamates complexes *S*,*S*-**1**, *R*,*S*-**2**, *R*,*R*-**3**, *S*,*R*-**4**, *S*,*S*-**5**, *R*,*S*-**6**, *R*,*R*-**7** and *S*,*R*-**8** suggests that HOMO orbitals are majorly localized at the dithiocarbamate moieties, however, LUMO orbitals show extended delocalization as shown in Figure 7 and Figure 8.

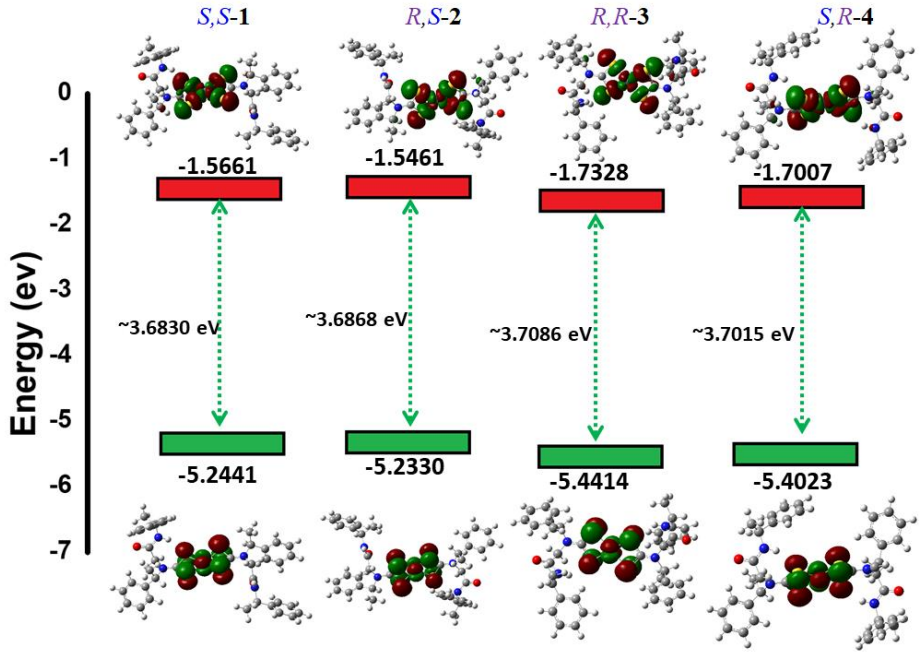

Figure 7. Comparison of the frontier molecular orbitals derived from DFT calculation at the B3LYP/LANL2DZ level for complexes *S,S*-**1,** *R,S*-**2,** *R,R*-**3** and *S,R*-**4**.

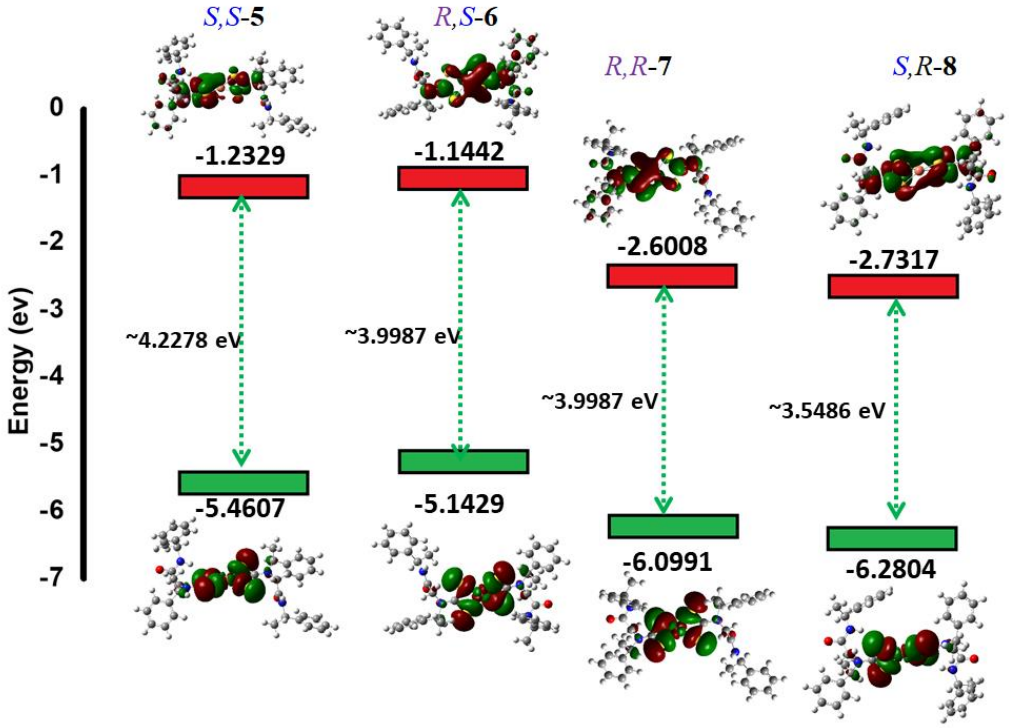

Figure 8. Comparison of the frontier molecular orbitals derived from DFT calculation at the B3LYP/LANL2DZ level for complexes *S,S*-**5,** *R,S*-**6,** *R,R*-**7** and *S,R*-**8**.

Table 8. Summary of Computational study performed on M^{II}-dithiocarbamate complexes *S,S*-**1,** *R,S*-**2,** *R,R*-**3,** *S,R*-**4,** *S,S*-**5,** *R,S*-**6,** *R,R*-**7** and *S,R*-**8**.

Entry	Energy (Hartree)	HOMO	LUMO	Energy Band Gap (ev)
S,S-**1**	-4943.25	-5.24418	-1.56112	3.6830
R,S-**2**	-4943.26	-5.23302	-1.54615	3.6868
R,R-**3**	-4943.25	-5.44146	-1.73282	3.7086
S,R-**4**	-4943.26	-5.40228	-1.70071	3.7015
S,S-**5**	-5075.41	-5.46078	-1.23295	4.2278
R,S-**6**	-5075.04	-5.14295	-1.14424	3.9987
R,R-**7**	-5075.01	-6.09916	-2.60087	3.4982
S,R-**8**	-5075.40	-6.28039	-2.73175	3.5486

The calculated HOMO-LUMO band gaps for all the newly synthesized complexes falls in the range of 3.5-4.2 eV which suggests non-conducting nature of the complexes. Further, the mapping of molecular electrostatic potential (MESP) of *S,S*-**1,** *R,S*-**2,** *R,R*-**3,** *S,R*-**4,** *S,S*-**5,** *R,S*-**6,** *R,R*-**7** and *S,R*-**8** clearly determines the projection of polar amide subunits in outward direction. Moreover, the existence of negative potential at the amidic oxygen and positive potential at the amidic proton can be visualized from the MESP diagrams shown in Figure 9. This, apparently suggest the ability of the molecules of *S,S*-**1,** *R,S*-**2,** *R,R*-**3,** *S,R*-**4,** *S,S*-**5,** *R,S*-**6,** *R,R*-**7** and *S,R*-**8** to offer secondary interactions with other molecules including biomolecules. It may be speculated that these molecules can interact with the biological molecules inside the cell required for improved biological activity through effective cellular membrane transportation towards the site of action.[36]

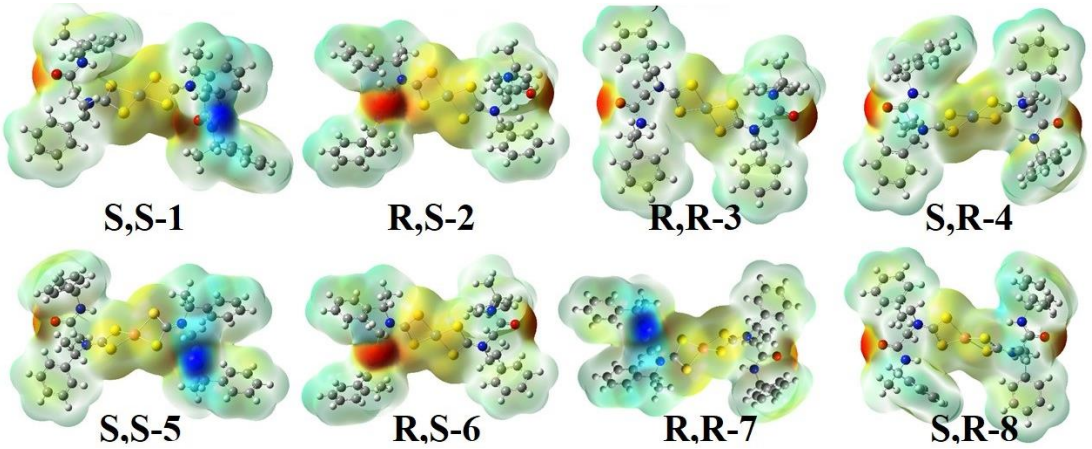

Figure 9. Representations of electron density from total SCF density (Isovalue= 0.0004; mapped with ESP)

6.4 Conclusions

In conclusion, a new series of monometallic N^{II}-/ Cu^{II}-dithiocarbamate complexes *S*,*S*-**1**, *R*,*S*-**2**, *R*,*R*-**3**, *S*,*R*-**4**, *S*,*S*-**5**, *R*,*S*-**6**, *R*,*R*-**7**, *S*,*R*-**8**, holding chirality in the ligand skeleton have been synthesized conveniently in a single step and characterized satisfactorily. The molecules of *R*,*S*-**2** have shown the propensity to form various intermolecular hydrogen bonding contacts as revealed by single crystal X-ray diffraction study which is further supported by the mapping of molecular electrostatic potential. All the compounds appear to be non-conducting nature and their HOMO-LUMO energy band gaps falls in the range of 3.5-4.2 eV. Interestingly, the thermal degradation of all the Ni^{II}/Cu^{II}-dithiocarbamate complexes gave a stable residual mass which corresponds to NiS/ CuS and thereby proves their suitability to serve as a single source precursor in the synthesis of metal-sulphide nanoparticle. In the light of the fact that chirality into nanostructured materials can be controlled deliberately either by employing different enantiomer templates or by the assistance of specific treatments, these compounds holding chirality in the ligand backbone would lead to development of chiral nanostructured materials.

6.5 Reference

1. (a) D. Coucouvanis, *Prog. Inorg. Chem*., **1979**, 26, 301; (b) P. I. Clemenson, *Coord. Chem. Rev.*, **1990**, 106, 171; (c) M. Bousseau, L. Valade, J. P. Legros, P. Cassoux, M. Garbaukas, L. V. Interrante, *J. Am. Chem. Soc.*; **1986**, 108, 1908; (d) P. Cassoux, L. Valade, H. Kobayashi, A. Kobayashi, R. A. Clark and A. E. Underhill, *Coord. Chem. Rev.*, **1991**, 110, 115.
2. (a) A. Clemenson, E. Fujiwara, H. Kobayashi, *Chem. Rev*., **2004**, 104, 5243. (b) P. Mathur, D. K. Rai, R. S. Ji, B. Pathak, S. Boodida, S. M. Mobin, *RSC Adv*., **2013**, 3, 26025; (c) A. T. Coomber, D. Beljonne, R. H. Friend, J. L. Bredas, A. Charlton, N. Robertson, A. E. Underhill, M. Kurmoo, P. Day, *Nature*, **1996**, 380, 144; (d) N. Singh, B. Singh, *Bull. Chem. Soc. Jpn.*, **2008**, 81, 262; (e) N. Singh, A. Prasad, R. K. Sinha, *Bull. Chem. Soc. Jpn*. **2009**, 82, 81.
3. (a) G. Hogarth, Prog. Inorg. Chem. **2005**, 53, 71; (b) G. Hogarth, Damian C. Onwudiwe, *Inorganics*, **2021**, 9, 70.
4. W. H. Tisdale, I. Williams, *Disinfectant*, US197296, **1934**.
5. (a) L. Kumar, A. Sarswat, N. Lal, V. L. Sharma, A. Jain, R. Kumar, V. Verma, J. P. Maikhuri, A. Kumar, P. K. Shukla, G. Gupta, *Eur. J. Med. Chem*., **2010**, 45, 817; (b) S. Jangir, V. Bala, N. Lal, L. Kumar, A. Sarswat, L. Kumar, B. Kushwaha, P. Singh, P. K. Shukla, J. P. Maikhuri, G. Gupta, V. L. Sharma, *Org. Biomol. Chem*. **2014**, 12, 3090; (c) T. F. Wood, J. H. Gardner, *J. Am. Chem. Soc*., **1941**, 63, 2741; (d) N. C. Kapa, G. G. Muccioli, G. Labar, J. H. Poupaert and D. M. Lambert, *J. Med. Chem*., **2009**, 52, 7310; (e) W. Huang, Y. Ding, Y. Miao, M. -Z. Liu, Y. Li and G. -F. Yang, *Eur. J. Med. Chem*., **2009**, 44, 3687.
6. C. S. I. Nobel, M. Kimland, B. Lind, S. Orrenius, A.F.G. Slater, *J. Biol. Chem*. **1995**, 270, 26202.
7. D. Buac, S. Schmitt, G. Ventro, F. R. Kona, Q. P. Dou, *Mini Rev. Med. Chem*., **2012**, 12, 1193.
8. T. Wang, Y. Fu, T. Huang, Y. Liu, M. Wu, Y. Yuan, S. Li, C. Li, *Molecules*, **2016**, 21, 1088.
9. L. Ronconi, C. Marzano, P. Zanello, M. Corsini, G. Miolo, C. Macca, A. Trevisan, D. J. Fregona, *Med. Chem*. **2006**, 49, 1648.
10. R. Schreck, B. Meier, D. N. Männel, W. Dröge, P.A. Baeuerle, *J. Exp. Med*., **1992**, 175, 1181.

11. V. Milacic, D. Chen, L. Ronconi, K. R. Landis-Piwowar, D. Fregona, Q.P. Dou, *Cancer Res*., **2006**, 66, 10478.
12. C. S. I. Nobel, D. H. Burgess, B. Zhivotovsky, M. J. Burkitt, S. Orrenius, A. F. Slater,*Chem. Res. Toxicol*. **1997**, 10, 636.
13. (a) B. A. Prakasam, M. Lahtinen, A. Peuronen, M. Muruganandham, E. Kolehmainen, E. Haapaniemi, M. Sillanpää, *Inorg. Chim. Acta*, **2015**, 425, 239; (b) B. A. Prakasam, M. Lahtinen, A. Peuronen, M. Muruganandham, E. Kolehmainen, E. Haapaniemi, M. Sillanpää, *Polyhedron*, **2014**, 81, 588.
14. (a) S. C. Han, K. W. Kim, H. J. Ahn, J. H. Ahn J. Y. Lee, *J. Alloys Compd*., **2003**, 361, 247; (b) A. Olivas, J. Cruz-Reyes, V. Petranovskii, M. Avalos, S. Fuentes, *J. Vac. Sci. Technol*., **1998**, 16A, 3515; (c) F. Atay, S. K. Ose, V. Bilgin, I. Akyuz. Turk, *J. Phys*. **2003**, 27, 285; (d) A. Roffey, N. Hollingsworth, H-U. Islam, M. Mercy, G. Sankar, C.R.A. Catlow, G. Hogarth, N.H. de Leeuw. *Nanoscale*, **2016**, 8, 11067.
15. (a) N. Kumar, N. Raman, A, Sundaresan, *J. Solid State Chem*., **2013**, 208, 103; (b) C. Gervas, S. Mlowe, M. P. Akerman, I. Ezekiel, T. Moyo, N. Revaprasadu, *Polyhedron*. **2017**, 122, 16.
16. (a) A. K. Sharma, *Thermochim. Acta* **1986**, 104, 339; (b) J. O. Hill, J. P. Murray, K. C. Patil, *Rev. Inorg. Chem*. **1994**, 14, 363.
17. J. A. Scott,; A. Angeloski, I. Aharonovich, C. J. Lobo, A. McDonagh, M. Toth, *Nanoscale*, **2018**, 10, 15669.
18. A. Roffey, N. Hollingsworth, H. U. Islam, M. Mercy, G. Sankar, C. R. Catlow, G. Hogarth, N.H. de Leeuw, *Nanoscale*, **2016**, 8, 11067.
19. (a) M. P. Motaung, D. C. Onwudiwe, L. Wei, C. Lou, *J. Phys. Chem. Solids*, **2021**, 160, 110319; (b) P. Roy, S. K. Srivastava, CrystEngComm, **2015**, 17, 7801.
20. (a) T. Aida, E. W. Meijer, S. I. Stupp, *Science*, **2012**, 335, 813; (b) V. K. Valev, J. J. Baumberg, C. Sibilia, T. Verbiest, *Adv. Mater*. **2013**, 25, 2517.
21. (a) Y. Zhou, M. Yang, K. Sun, Z. Tang, N. A. Kotov, *J. Am. Chem. Soc*., **2010**, 132, 6006; (b) K. E. Shopsowitz, H. Qi, W. Y. Hamad, M. MacLachlan, *J. Nature*, **2010**, 468, 422; (c) J. Zhu, H. Peng, A. F. Marshall, D. M. Barnett, W. D. Nix, Y. Cui, *Nat. Nanotechnol*., **2008**, 3, 477.
22. (a) Y. Wang, J. Xu, Y. Wang, H. Chen, *Chem. Soc. Rev*., **2013**, 42, 2930; (b) H. Qiu, S. Che, *Chem. Soc. Rev*. **2011**, 40, 1259.

23. (a) J. M. Slocik, A. O. Govorov, R. R. Naik, *Nano Lett*., **2011**, 11, 701; (b) C.-L. Chen, N. L. Rosi, *Angew. Chem*., **2010**, 49, 1924.
24. (a) Z. Li, Z. Zhu, W. Liu, Y. Zhou, B. Han, Y. Gao, Z. Tang, *J. Am. Chem. Soc*. **2012**, 134, 3322; (b) G. Shemer, O. Krichevski, G. Markovich, T. Molotsky, I. Lubitz, A. B. Kotlyar, *J. Am. Chem. Soc*., **2006**, 128, 11006.
25. (a) T. Delclos, C. Aimé, E. Pouget, A. Brizard, I. Huc, M.-H. Delville, R. Oda,V *Nano Lett*., **2008**, 8, 1929; (b) R.-Y. Wang, H. Wang, X. Wu, Y. Ji, P. Wang, Y. Qu, T.-S. Chung, *Soft Matter*, **2011**, 7, 8370.
26. (a) J. H. Jung, S.-H. Lee, J. S. Yoo, , K. Yoshida, T. Shimizu, S. Shinkai, *Chem. Eur. J*. **2003**, 9, 5307; (b) M. Llusar, C. *Chem. Mater*., **2008**, 20, 782−820.
27. (a) C. Li, K. Deng, Z. Tang, L. Jiang, *J. Am. Chem. Soc*. **2010**, 132, 8202. (b) J. George, K. G. Thomas, *J. Am. Chem. Soc*. **2010**, 132, 2502; (c) Y. Ma, Z. Cao, J. Hao, J. Zhou, Z. Yang, Y. Yang, J. Wei, *J. Phys. Chem*., **2020**, 124, 24306.
28. (a) Q. Chen, J. K. Whitmer, S. Jiang, S. C. Bae, E. Luijten, S. Granick, *Science*, **2011**, 331, 199−202; (b) H. Wang, J. -C. Wu, Y. Shen, G. Li, Z. Zhang, G. Xing, D. Guo, D. Wang, Z. Dong, T. Wu, *J. Am. Chem. Soc*. **2010**, 132, 15875.
29. H. -E. Lee, H. -Y. Ahn, J. Mun, Y. Y. Lee, M. Kim, N. H. Cho, K. Chang, W. S. Kim, J. Rho, K. T. Nam, *Nature*, **2018**, 556, 360.
30. L. Zhu, X. Li, S. Wu, K. T. Nguyen, H, Yan, H, Ågren, Y. Zhao, *J. Am. Chem. Soc*., **2013**, 135, 9174.
31. G. Gonza´lez-Rubio, J. Mosquera, V. Kumar, A. Pedrazo-Tardajos, P. Llombart, D. M. Solı´s, I. Lobato, E. G. Noya, A. Guerrero-Martı´nez, J. M. Taboada, F. Obelleiro, L. G. MacDowell, S. Bals, L. M. Liz-Marza´n, *Science*, **2020**, 368, 1472.
32. CrysAlispro program (Version 1.171.37.33 Agilent Technologies, **2014**.
33. O. V. Dolomanov, L. J. Bourhis, R. J. Gildea J. A. K. , Howard, H. Puschmann, *J. Appl.Cryst*., **2009**, 42, 339-345
34. G. M. Sheldrick,SHELXL-97: program for crystal structure refinement, University of Göttingen, Göttingen, Germany, **1997**.
35. M. J. Frisch, G. W. Trucks, H. B. Schlegel, G. E. Scuseria, M. A. Robb, J. R. Cheeseman, G. Scalmani, V. Barone, G. A. Petersson, H. Nakatsuji, X. Li, M. Caricato, A. V. Marenich, J. Bloino, B. G. Janesko, R. Gomperts, B. Mennucci, H. P. Hratchian, J. V. Ortiz, A. F. Izmaylov, J. L. Sonnenberg, D. Williams-Young, F. Ding, F. Lipparini, F. Egidi, J. Goings, B. Peng, A. Petrone, T.

Henderson, D. Ranasinghe, V. G. Zakrzewski, J. Gao, N. Rega, G. Zheng, W. Liang, M. Hada, M. Ehara, K. Toyota, R. Fukuda, J. Hasegawa, M. Ishida, T. Nakajima, Y. Honda, O. Kitao, H. Nakai, T. Vreven, K. Throssell, J. A. Montgomery, Jr, J. E. Peralta, F. Ogliaro, M. J. Bearpark, J. J. Heyd, E. N. Brothers, K. N. Kudin, V. N. Staroverov, T. A. Keith, R. Kobayashi, J. Normand, K. Raghavachari, A. P. Rendell, J. C. Burant, S. S. Iyengar, J. Tomasi, M. Cossi, J. M. Millam, M. Klene, C. Adamo, R. Cammi, J. W. Ochterski, R. L. Martin, K. Morokuma, O. Farkas, J. B. Foresman, D. J. Fox, Gaussian, Inc. Wallingford CT, **2016.**

36. (a) C. J. Savani, H. Roy, S. K. Verma, D. R. Vennapu, V. K. Singh, *Appl. Organomet. Chem.*, **2021**, 35, e6137; (b) C. J. Savani, D. R.Vennapu, H. Roy, V. K. Singh, *J. Organomet. Chem.*, **2021**, 950, 121983-121989; (c) V. K. Singh, V. Pillai, S. K. Patel, L. Buch, *ChemistrySelect*, **2019**, 4, 8689; (d) V. Pillai, S. K. Patel, L. Buch, V. K. Singh, *Appl. Organometal Chem*., **2018**, 32, e4559.
37. (a) A. Pete, Ajibade, P. Fartisincha, Andrew, N. L. Botha, N. Solomane, *Molecules*., **2020**, 25, 3584; (b) S. K. Patel, K. Kolte, C. J. Savani, P. Raghavaiah, D. Dave, A. A. Isab, D. Mistry, D. Suthar, V. K. Singh, *Inorganica Chimica Acta*, **2022**, 543, 121139.

6.6 Annexures

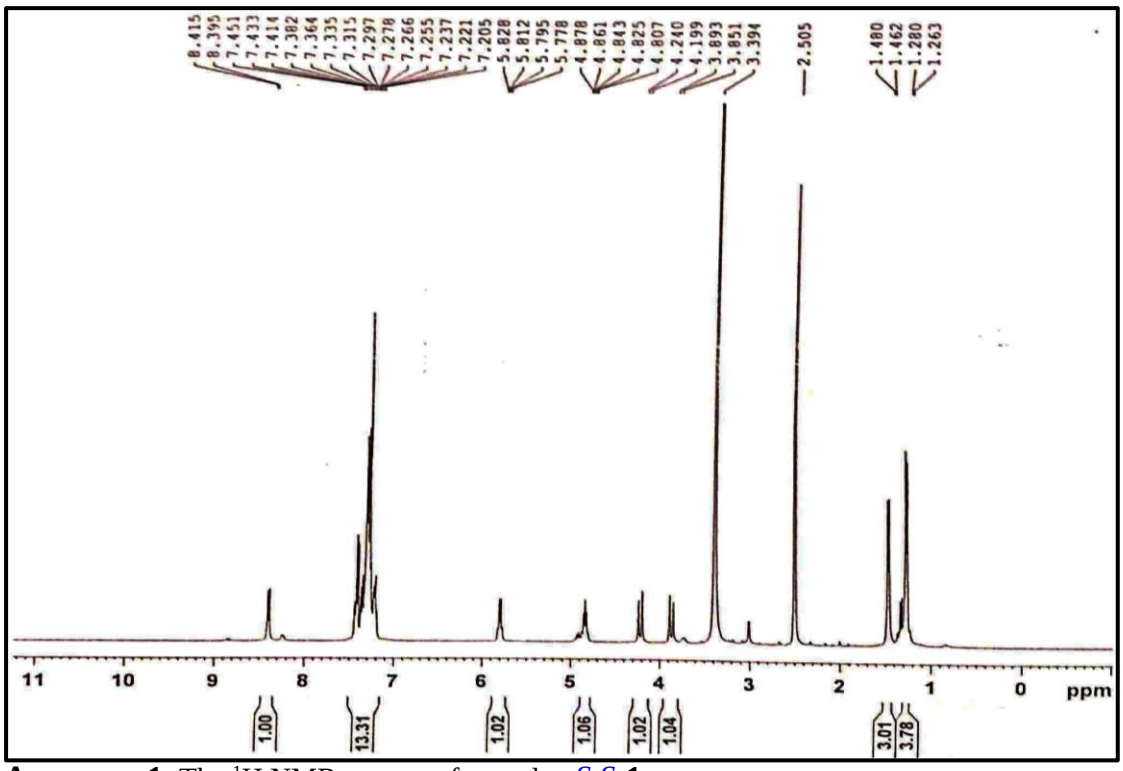

Annexure 1. The ^{1}H NMR spectra of complex *S*,*S*-**1**.

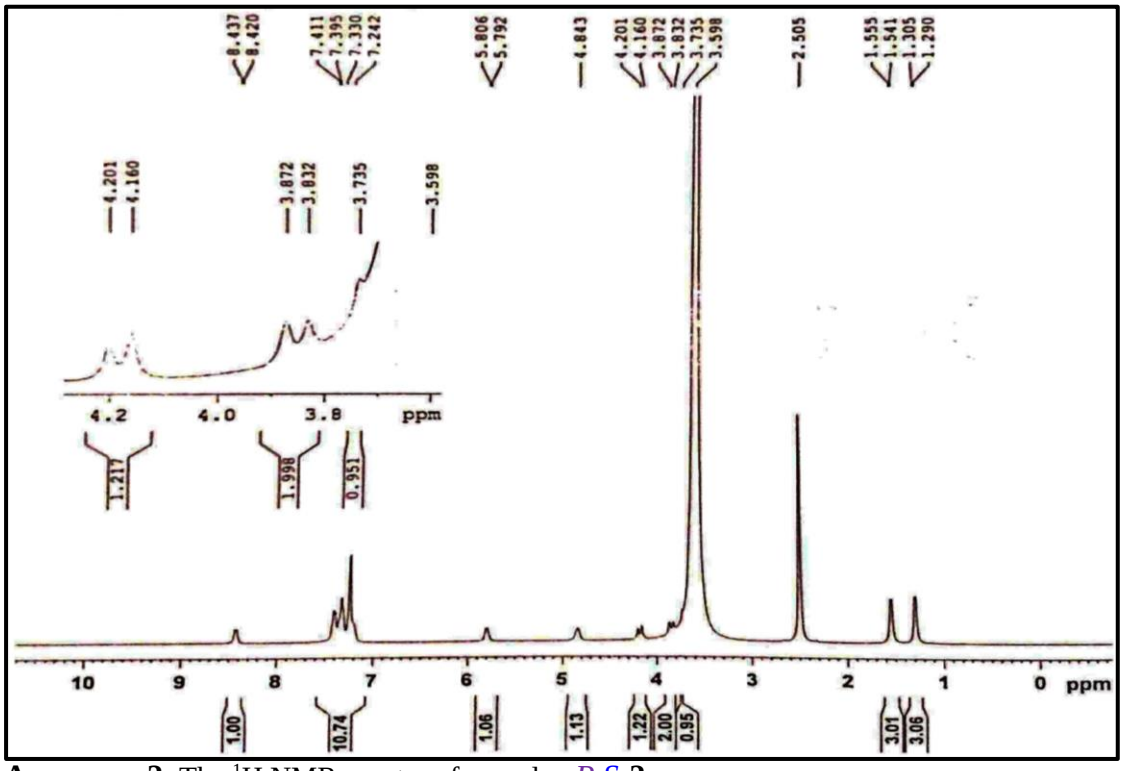

Annexure 2. The ^{1}H NMR spectra of complex *R*,*S*-**2**.

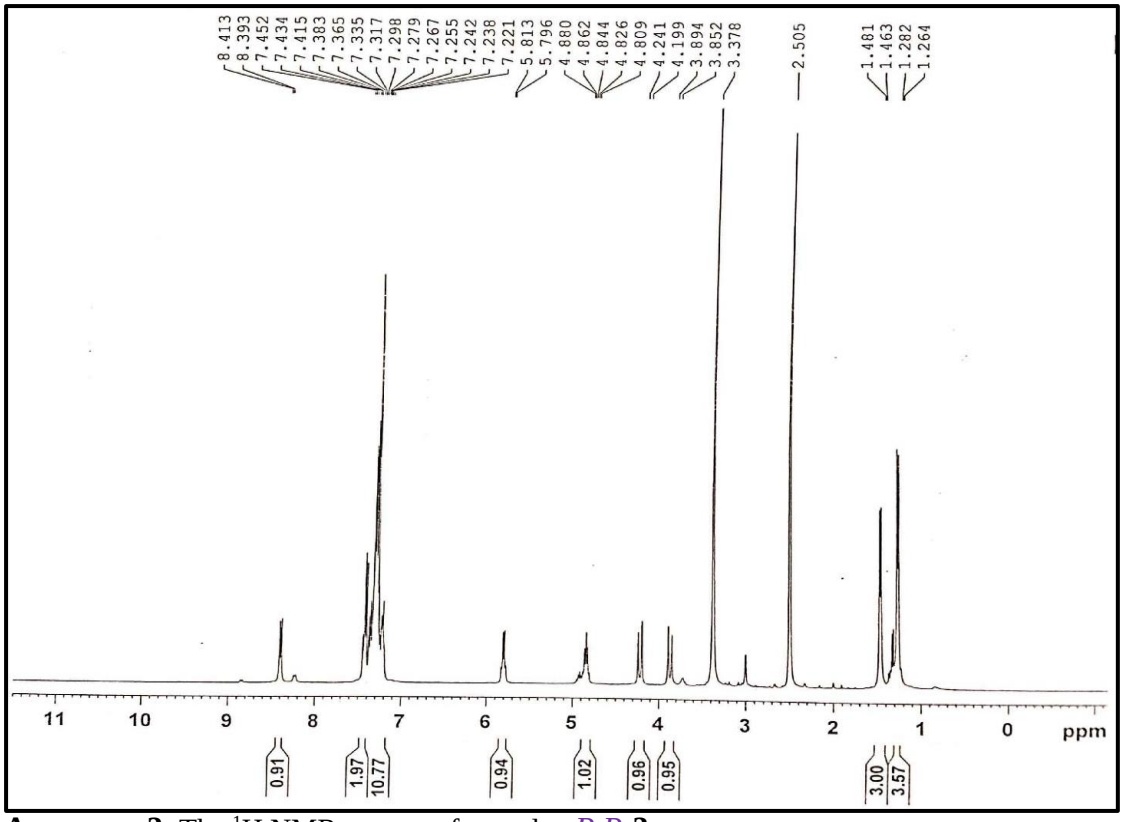

Annexure 3. The ^{1}H NMR spectra of complex *R*,*R*-**3**.

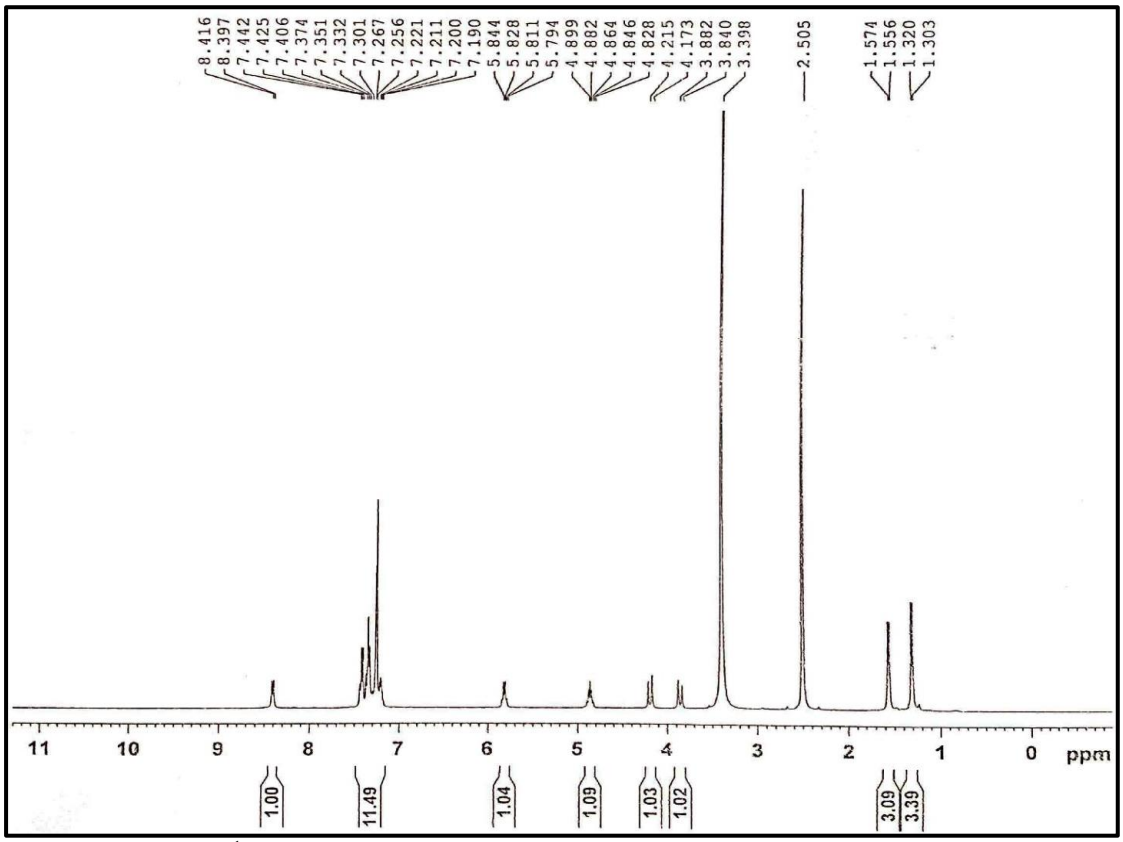

Annexure 4. The ^{1}H NMR spectra of complex *S*,*R*-**4**.

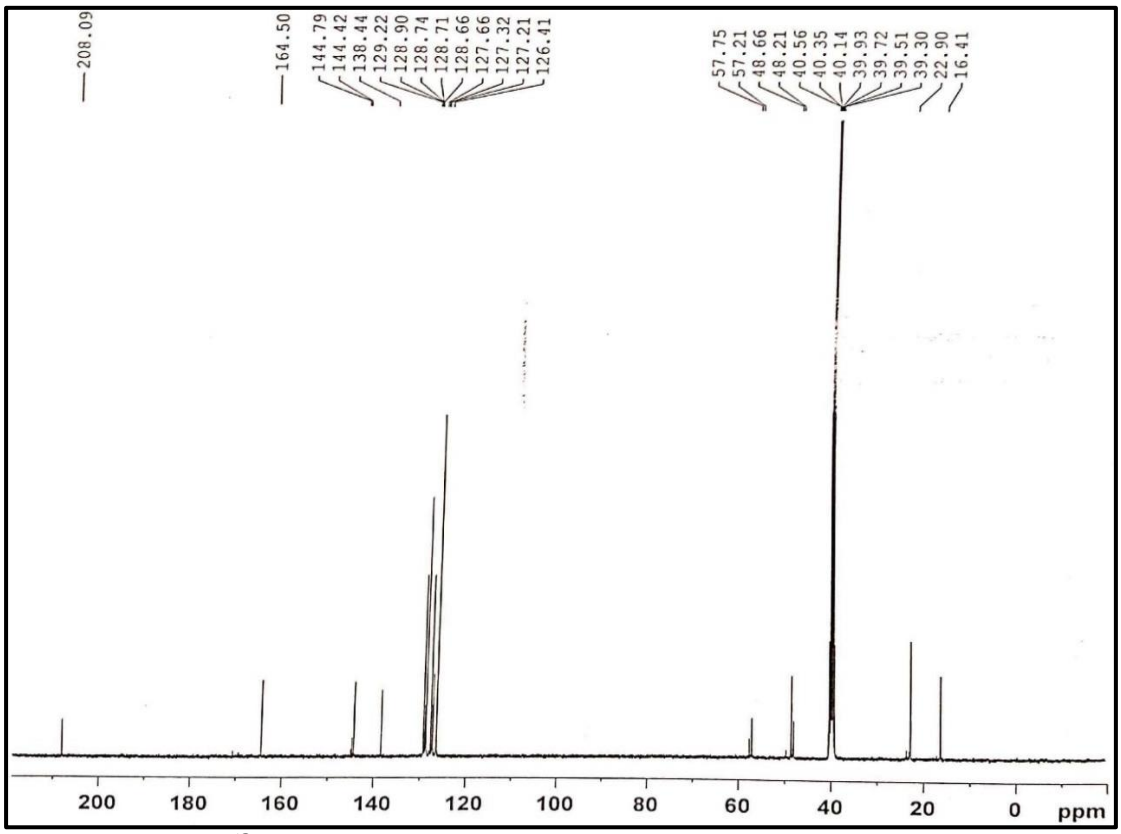

Annexure 5. The ^{13}C NMR spectra of *S*,*S*-**1**

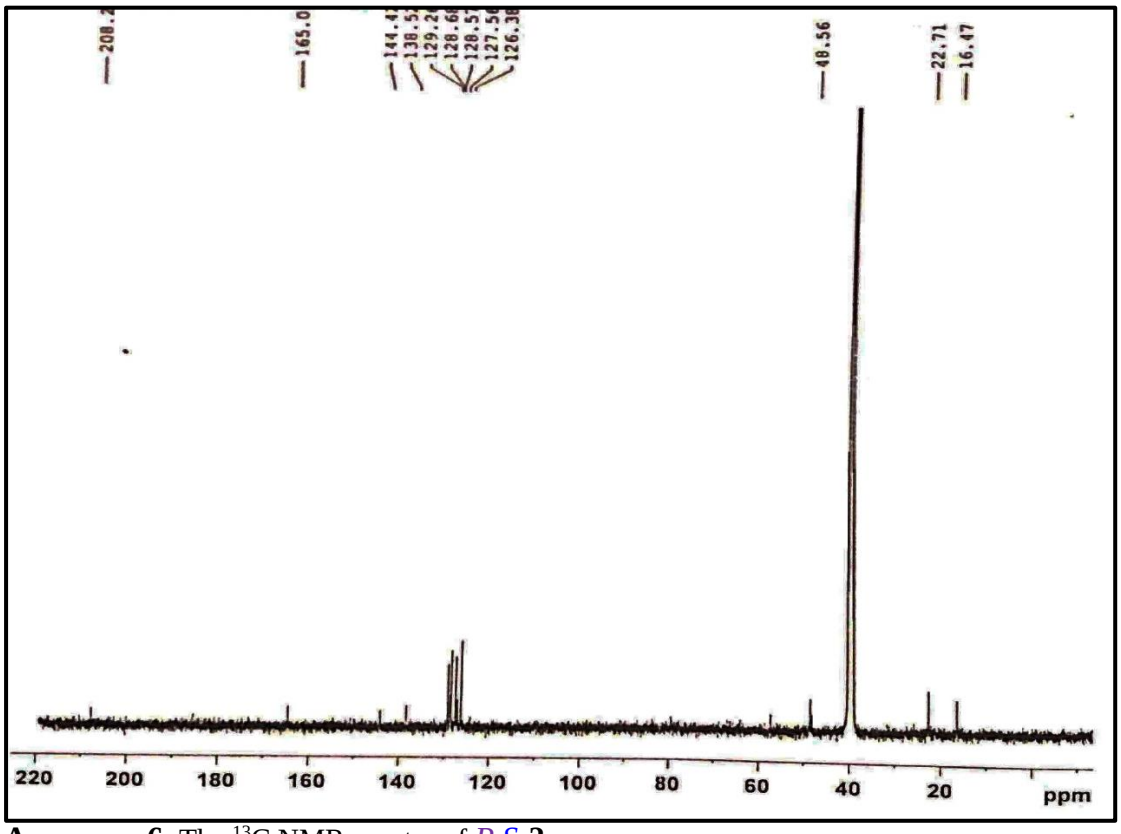

Annexure 6. The ^{13}C NMR spectra of *R*,*S*-**2**

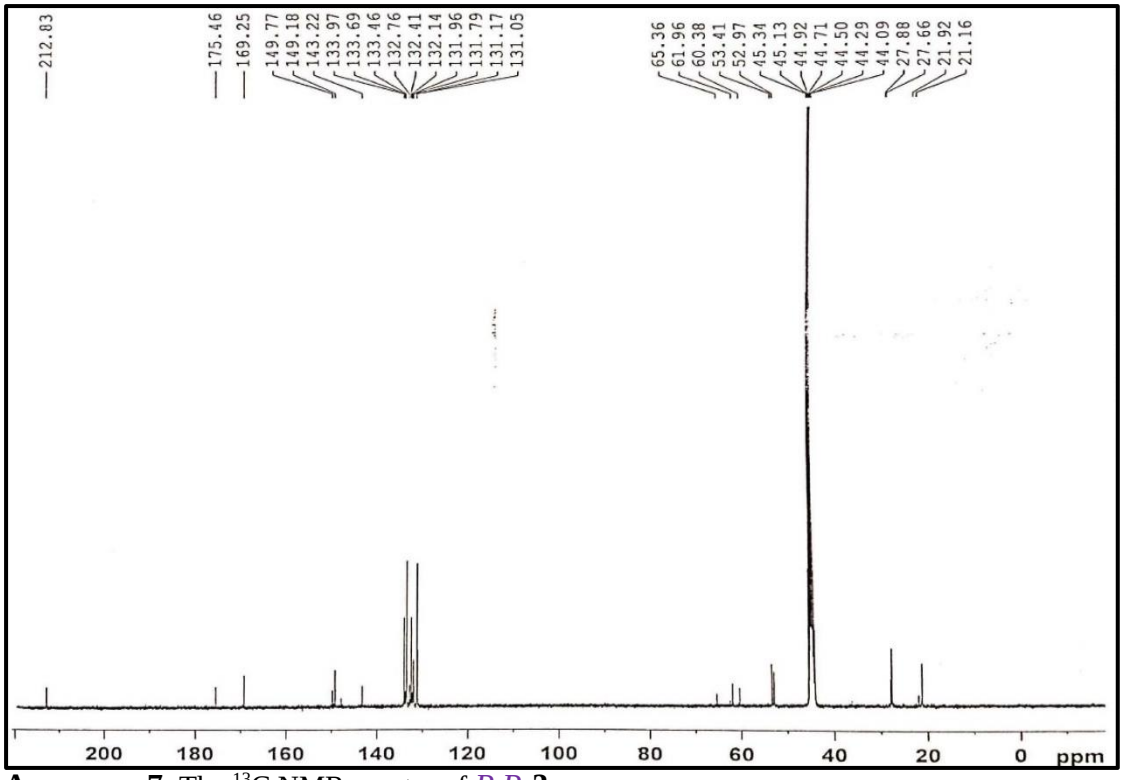

Annexure 7. The ^{13}C NMR spectra of *R,R*-**3**

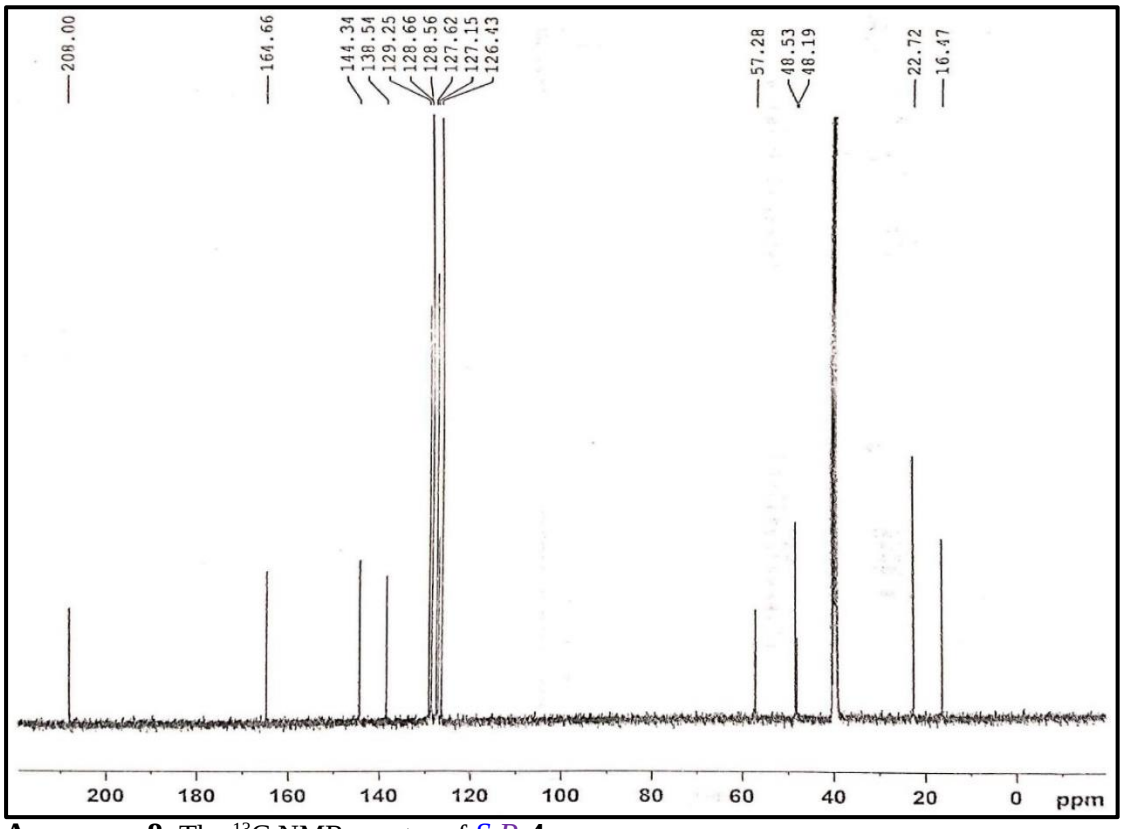

Annexure 8. The ^{13}C NMR spectra of *S,R*-**4**

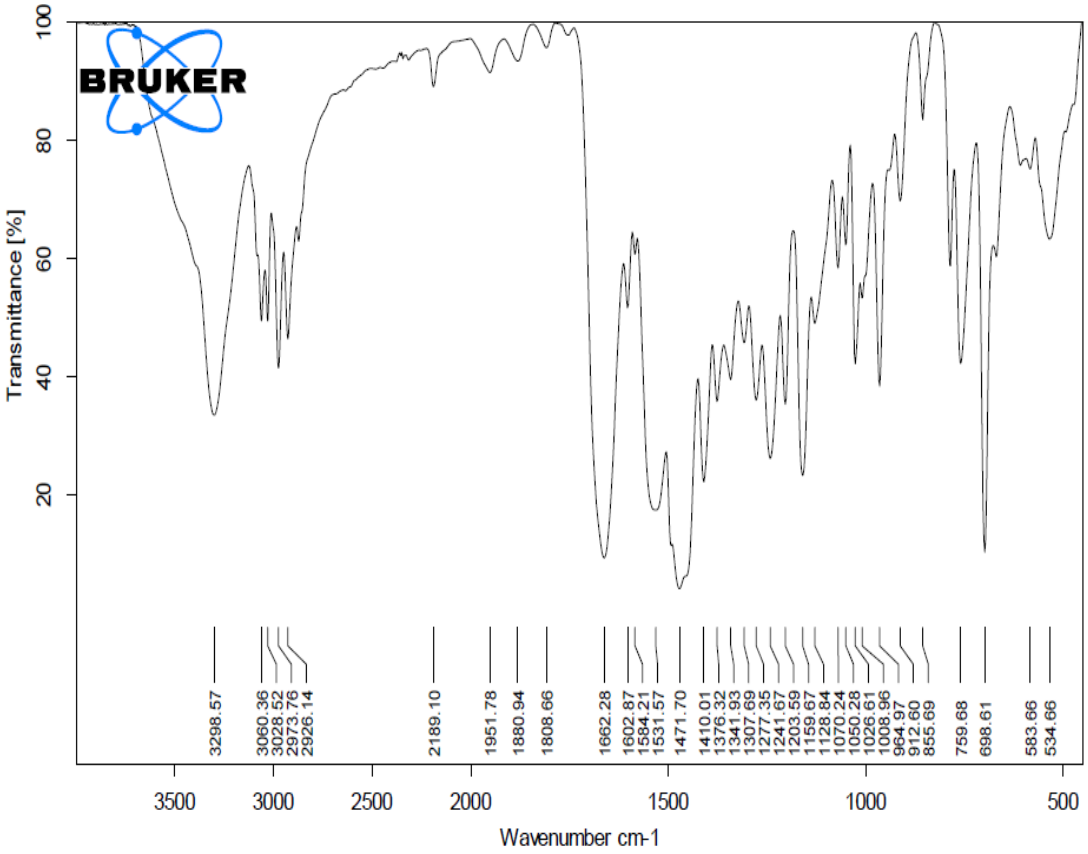

Annexure 9. IR spectrum of *S*,*S*-**1**.

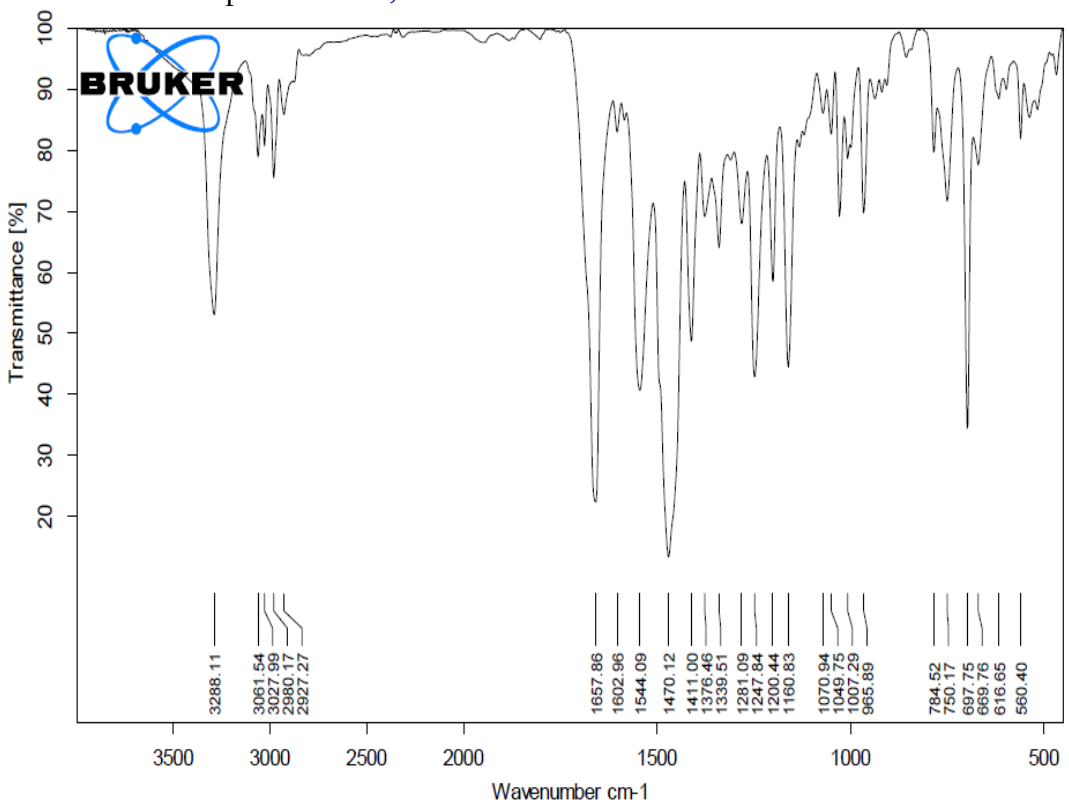

Annexure 10. IR spectrum of *R*,*S*-**2**.

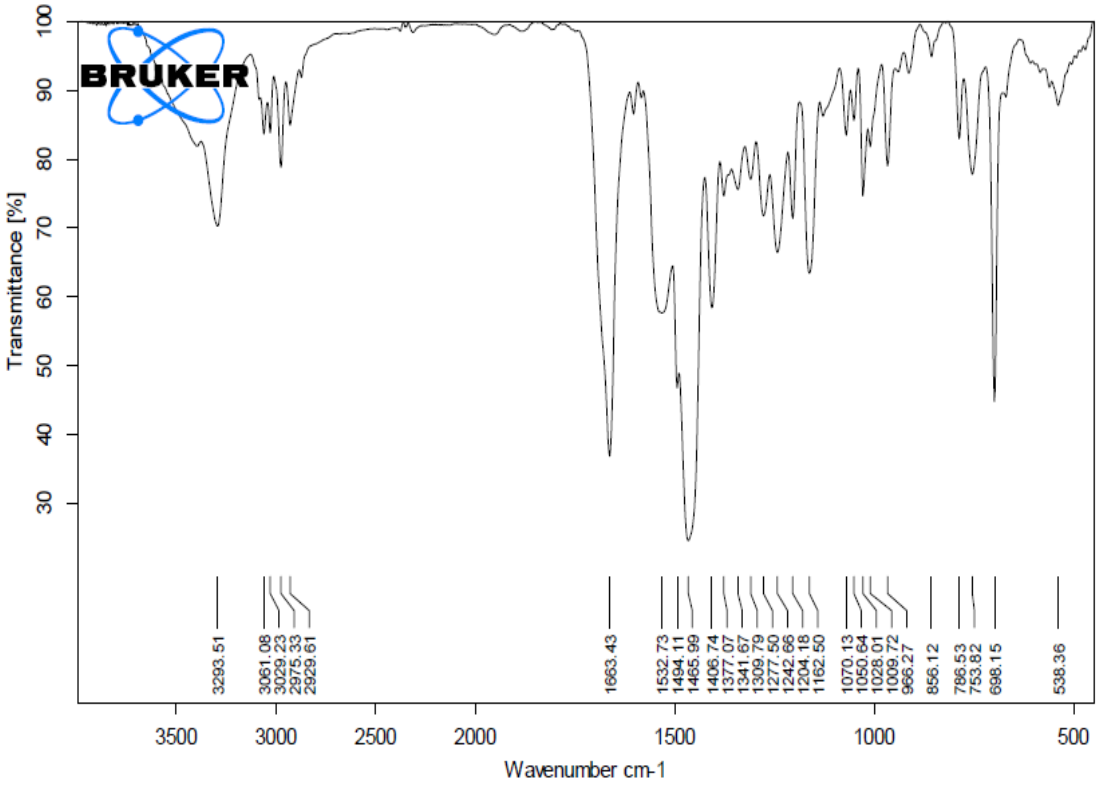

Annexure 11. IR spectrum of *R*,*R*-**3**.

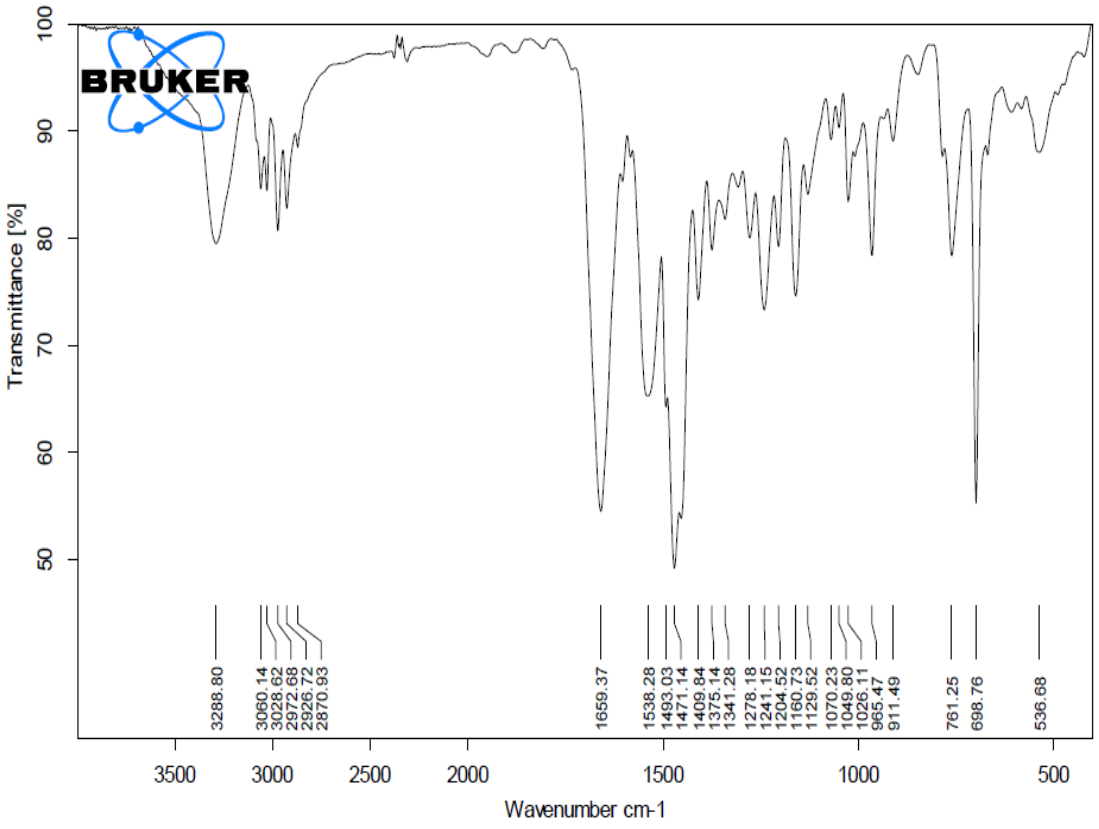

Annexure 12. IR spectrum of *S*,*R*-**4**.

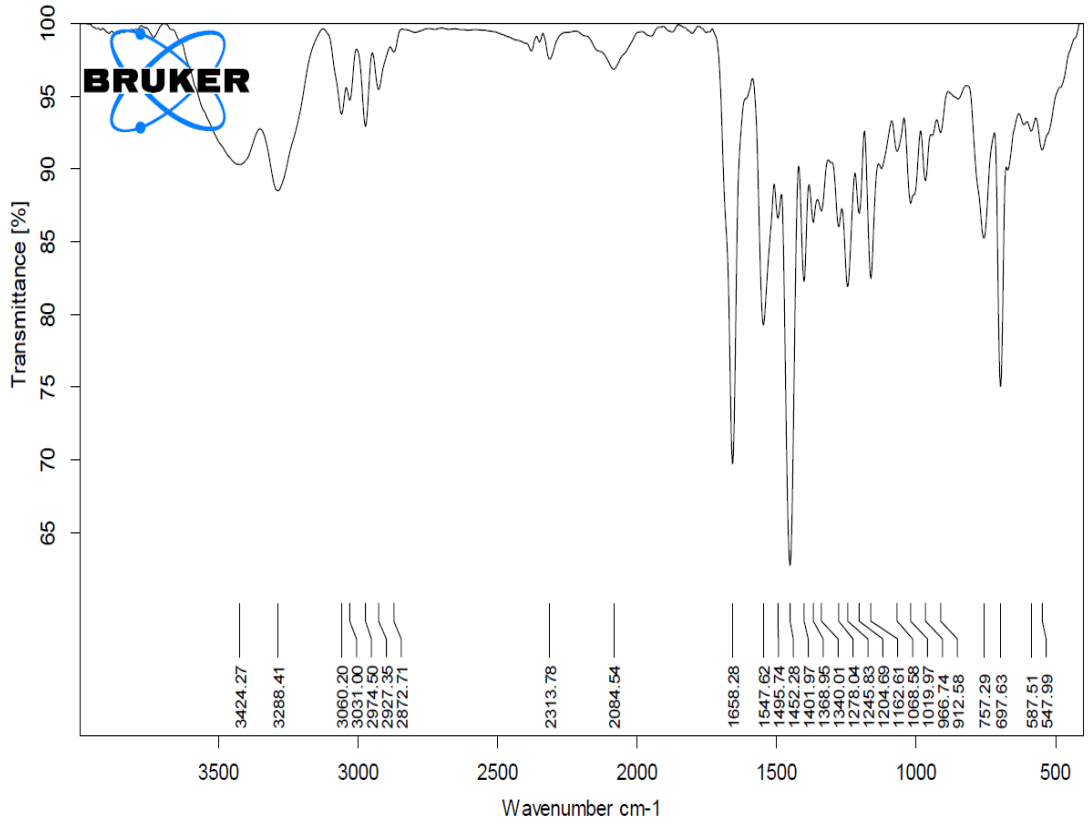

Annexure 13. IR spectrum of *S*,*S*-**5**.

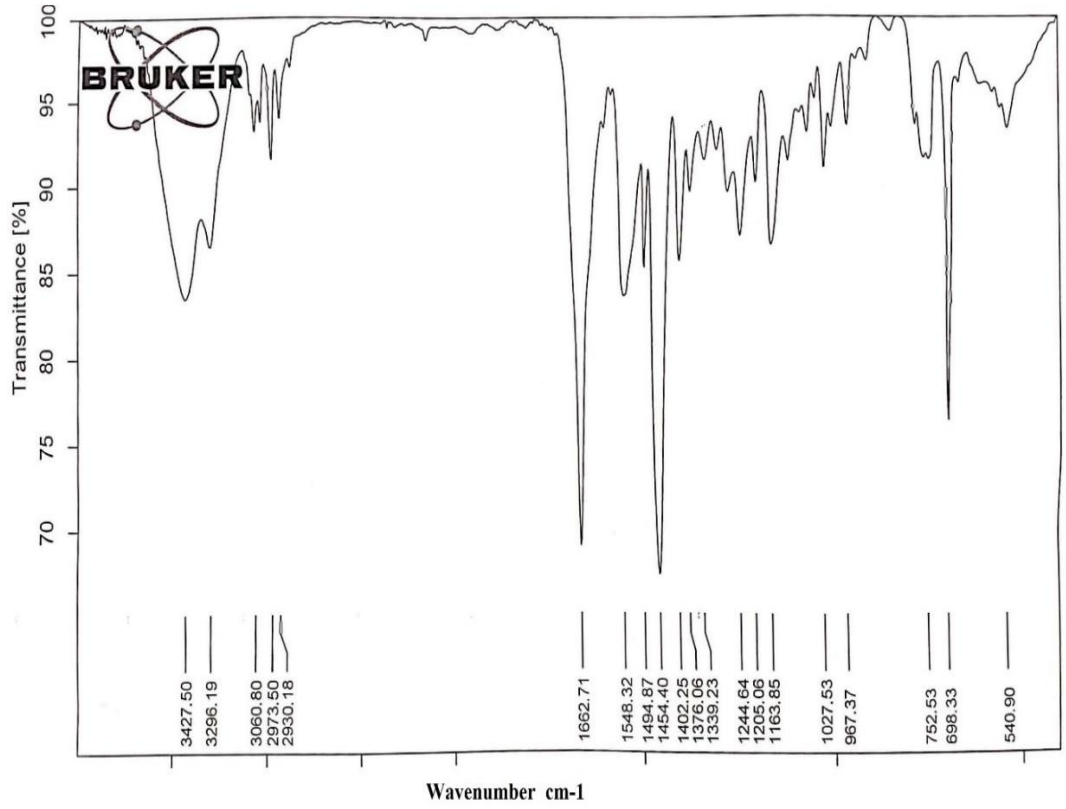

Annexure 14. IR spectrum of *R*,*S*-**6**.

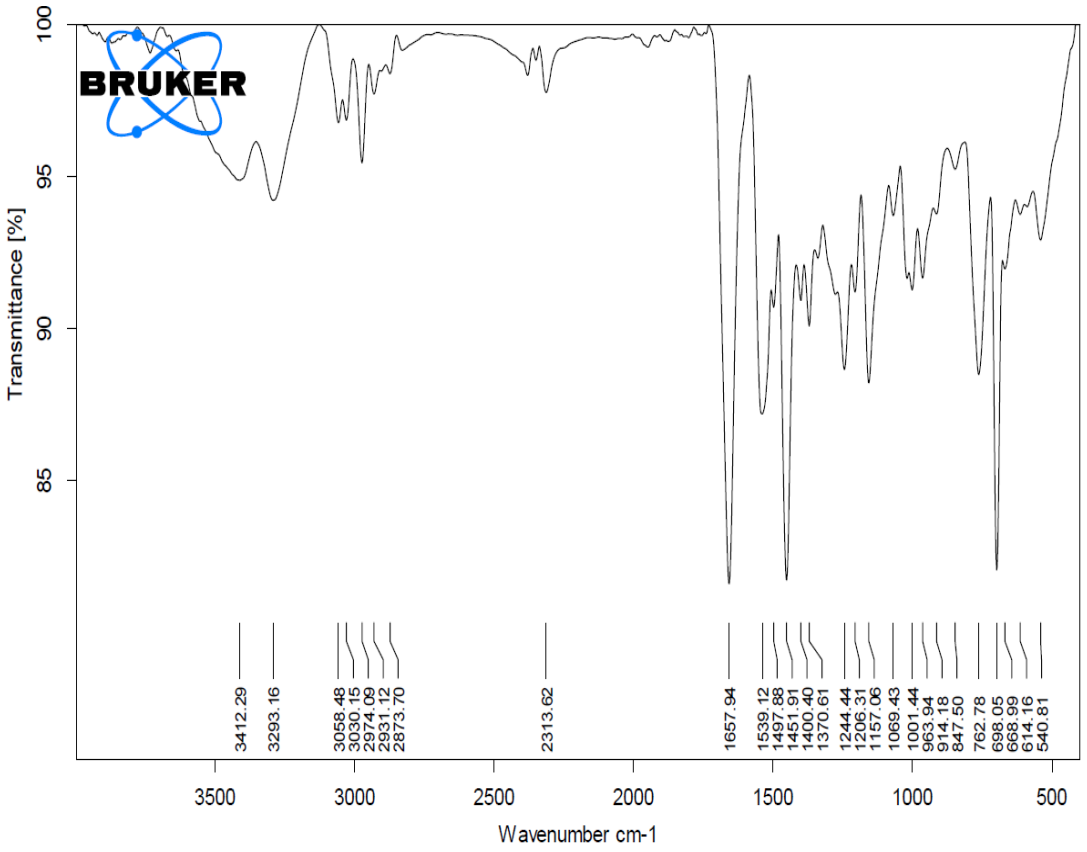

Annexure 15. IR spectrum of *R*,*R*-**7**.

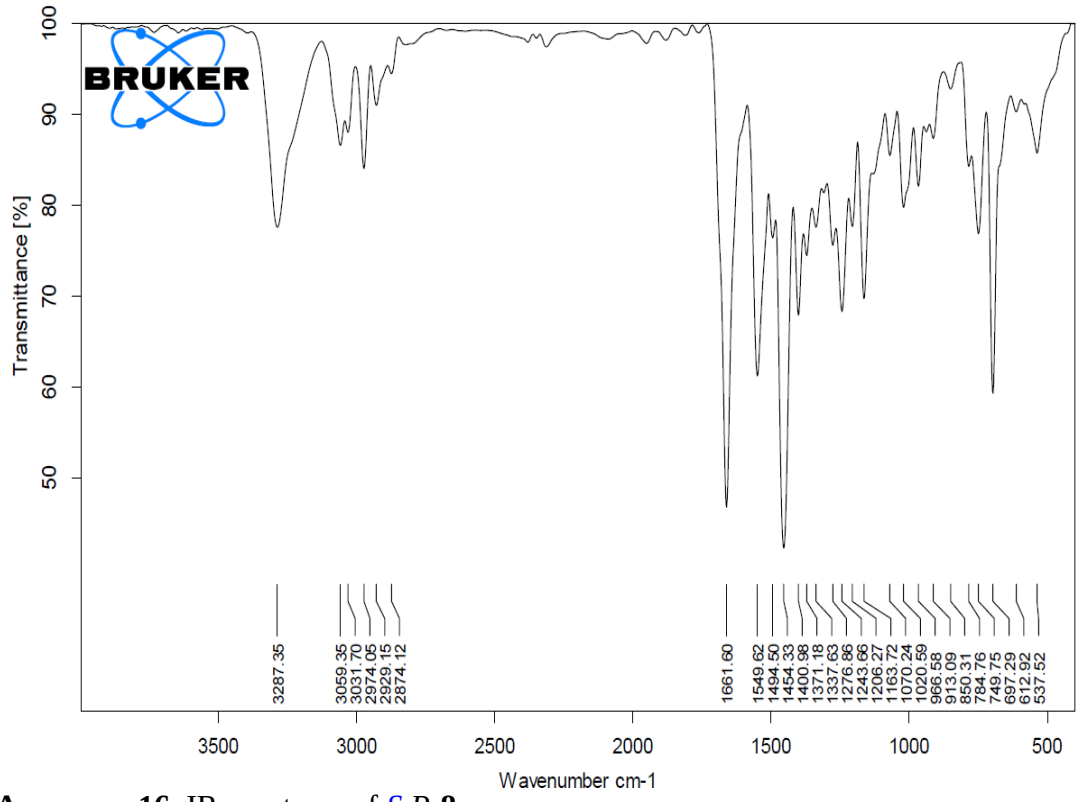

Annexure 16. IR spectrum of *S*,*R*-**8**.